The Astrophysical Journal, 658:1264–1288, 2007 April 1
© 2007. The American Astronomical Society. All rights reserved. Printed in U.S.A.

THE FREQUENCY OF MID-INFRARED EXCESS SOURCES IN GALACTIC SURVEYS

B. Uzpen,[1] H. A. Kobulnicky,[1] A. J. Monson,[1] M. J. Pierce,[1] D. P. Clemens,[2] D. E. Backman,[3] M. R. Meade,[4] B. L. Babler,[4] R. Indebetouw,[5] B. A. Whitney,[6] C. Watson,[7] M. G. Wolfire,[8] R. A. Benjamin,[9] S. Bracker,[4] T. M. Bania,[2] M. Cohen,[10] C. J. Cyganowski,[4] K. E. Devine,[4] F. Heitsch,[11] J. M. Jackson,[2] J. S. Mathis,[4] E. P. Mercer,[2] M. S. Povich,[4] J. Rho,[12] T. P. Robitaille,[13] M. Sewilo,[4] S. R. Stolovy,[12] D. F. Watson,[4] M. J. Wolff,[6] and E. Churchwell[4]

Received 2006 May 17; accepted 2006 December 8

ABSTRACT

We have identified 230 Tycho-2 Spectral Catalog stars that exhibit 8 μm mid-IR extraphotospheric excesses in the *MSX* and *Spitzer* GLIMPSE surveys. Of these, 183 are either OB stars earlier than B8 in which the excess plausibly arises from a thermal bremsstrahlung component or evolved stars in which the excess may be explained by an atmospheric dust component. The remaining 47 stars have spectral classifications B8 or later and appear to be main-sequence or late pre–main-sequence objects harboring circumstellar disks. Six of the 47 stars exhibit multiple signatures characteristic of pre–main-sequence circumstellar disks, including emission lines, near-IR *K*-band excesses, and X-ray emission. Approximately one-third of the remaining 41 sources have emission lines suggesting relative youth. We modeled the excesses in 26 stars having two or more measurements in excess of the expected photospheres as single-component blackbodies. We determine probable disk temperatures and fractional IR luminosities in the range $191\ \mathrm{K} < T < 787\ \mathrm{K}$ and $3.9 \times 10^{-4} < L_{\mathrm{IR}}/L_* < 2.7 \times 10^{-1}$. The majority of our modeled sample (14 stars) have $10^{-3} < L_{\mathrm{IR}}/L_* < 10^{-2}$ and are consistent with either transition disks or massive debris disks. These objects have fractional IR luminosities and temperatures between those of β Pic–type debris disk systems ($L_{\mathrm{IR}}/L_* \leq 10^{-3}$) and Class II pre–main-sequence systems ($L_{\mathrm{IR}}/L_* \simeq 10^{-1}$). We estimate a lower limit on the fraction of Tycho-2 Spectral Catalog main-sequence stars having mid-IR, but not near-IR, excesses to be $1.0\% \pm 0.3\%$.

Subject headings: circumstellar matter — planetary systems

1. INTRODUCTION

The formation of planetary systems is one of the major unsolved problems in modern-day astronomy. A necessary step in understanding planet formation is understanding the circumstellar disks in which the planets form (Lada & Wilking 1984). During evolution of a Class II[14] pre–main-sequence star (T Tauri or Herbig Ae/Be star), the original optically thick circumstellar disk dissipates as a star approaches the main sequence. These disks reradiate stellar energy at longer wavelengths (e.g., Zuckerman 2001). Because of this reradiation, pre–main-sequence stars are easily detected in the far-IR. When the primordial disk is nearly depleted, the star becomes a Class III pre–main-sequence star. After the initial primordial disk clears nearly all of its gas and dust, a new disk can form (e.g., Lagrange et al. 2000). This disk is not due to the initial collapse of the interstellar cloud, but rather it is a second-generation structure produced by fragmentation of planetesimals that formed in the original protoplanetary disk. These second-generation disks are composed primarily of dust and are known as debris disks (e.g., Backman & Paresce 1993).

The detection of an excess in the infrared does not necessarily imply the presence of a disk, but investigations of infrared excesses often reveal the existence and nature of disks. The fractional infrared luminosity, L_{IR}/L_*, can be used to differentiate between protoplanetary and debris disks. Protoplanetary disk systems have $L_{\mathrm{IR}}/L_* \leq 10^{-1}$, while debris disk systems have $L_{\mathrm{IR}}/L_* \simeq 10^{-3}$ (Lagrange et al. 2000). Debris disk prototypes are the 200 ± 100 Myr old Vega system (Barrado y Navascués 1998), which has a far-IR excess at $\lambda \geq 24$ μm (Su et al. 2005), and the 20 ± 10 Myr (Barrado y Navascués et al. 1999) old β Pictoris system, which has an excess at mid- and far-IR wavelengths ($\lambda > 4.5$–10 μm; Backman et al. 1992). Sylvester et al. (1996) investigated 23 main-sequence stars exhibiting large fractional infrared excesses at far-IR wavelengths and found that 9 of these sources exhibited near-IR excesses ($\lambda < 3$ μm), yielding similar near-IR colors to pre–main-sequence stars. The stars exhibiting near-IR excesses had greater fractional infrared luminosities than typical Vega-like systems, consistent with the presence of remnants from the original protoplanetary disk. The wavelength where the excess first appears provides an indication of the nature and evolutionary status of the disk. Sylvester et al. (1996) found that the stars that exhibited an excess only at $\lambda > 3.5$ μm were more similar to Vega-like systems. The largest fractional infrared luminosities appear at the shortest wavelengths and indicate the most massive and optically thick disks, while the smallest excesses appear only at long wavelengths and are signatures of debris disks. A complete evolutionary progression from protoplanetary disk systems to Vega-like disk systems has yet to be determined. Dusty debris may cause the IR excess at any point after planetesimals have formed and the disks have cleared their

[1] Department of Physics and Astronomy, University of Wyoming, Laramie, WY.
[2] Institute for Astrophysical Research, Boston University, Boston, MA.
[3] SOFIA, NASA-Ames Research Center, Moffett Field, CA.
[4] Department of Astronomy, University of Wisconsin, Madison, WI.
[5] Department of Astronomy, University of Virginia, Charlottesville, VA.
[6] Space Science Institute, Boulder, CO.
[7] Department of Physics, Manchester College, North Manchester, IN.
[8] Department of Astronomy, University of Maryland, College Park, MD.
[9] Physics Department, University of Wisconsin, Whitewater, WI.
[10] Radio Astronomy Laboratory, University of California, Berkeley, CA.
[11] Department of Astronomy, University of Michigan, Ann Arbor, MI.
[12] *Spitzer* Science Center, California Institute of Technology, Pasadena, CA.
[13] School of Physics and Astronomy, University of St. Andrews, North Haugh, St Andrews, Fife, UK.

[14] Using the stellar formation classes of Wilking et al. (1989), Class I objects are accreting protostars, Class II are pre–main-sequence stars with circumstellar disks, and Class III are pre–main-sequence stars with their circumstellar disk nearly dissipated.

gaseous component, a process that takes 3–30 Myr (Meyer et al. 2007 and references therein).

The detection of dust around main-sequence stars provides insight into the planetary formation process. Aumann et al. (1984) reported the first detection of an IR excess owing to dust in the Vega system, and this excess was later explained as a debris disk. Infrared excesses are the signatures that have allowed the *Infrared Astronomical Satellite* (*IRAS*), *Infrared Space Observatory* (*ISO*), and *Spitzer Space Telescope* (Werner et al. 2004) to identify nearby stars with disk systems, including protoplanetary disks and debris disks (Werner et al. 2006; Lagrange et al. 2000; Mannings & Barlow 1998; Backman & Paresce 1993 and references therein). Using the *IRAS* Point Source Catalog matched with the SAO catalog, Oudmaijer et al. (1992) identified 462 stars that exhibited infrared excesses based on photometric colors. This same technique was utilized by Clarke et al. (2005), in which the *Midcourse Space Experiment* (*MSX*; Egan et al. 2003) catalog was matched with the Tycho-2 Spectral Catalog to identify 1938 sources that exhibited an infrared excess based on photometric colors. Both the Oudmaijer et al. (1992) and Clarke et al. (2005) samples provide a wealth of sources to further investigate the nature of the stellar excesses. Understanding the nature of the excess allows statistical surveys into the frequency of occurrence of circumstellar material located around stars. At least 15% of nearby A–K main-sequence stars have dusty debris disks that were detectable to *IRAS* and *ISO* sensitivities in the far-infrared (Meyer et al. 2007; Lagrange et al. 2000; Backman & Paresce 1993). Plets & Vynckier (1999) found the excess fraction for both main-sequence stars and their descendants also to be $\sim$13% $\pm$ 10% at 60 μm, and Bryden et al. (2006) found an excess fraction of 2% $\pm$ 2% at 24 μm, for main-sequence field FGK stars with $L_{\rm IR}/L_* \geq 10^{-4}$.

Excesses at mid-IR wavelengths are much less common for main-sequence stars (Meyer et al. 2007). Aumann & Probst (1991) investigated 548 nearby main-sequence stars using 12 μm measurements from *IRAS*, but out of the 60 stars with possible $V - [12]$ excesses targeted for ground-based follow-up, only β Pictoris and ζ Leporis exhibited genuine excesses once confusing sources within the large *IRAS* beam were excised. Fajardo-Acosta et al. (2000) investigated 2834 *IRAS* sources, of which 296 were main-sequence B9 through M stars, and found eight possible 12 μm excesses. Stars that exhibit a mid-infrared excess have characteristic disk temperatures of 200–1000 K and dust within a few AU of the star, similar to our asteroid belt. By comparison, long-wavelength excesses have cooler $\sim$100 K dust located farther from the central star and are more comparable to the Kuiper Belt. The warmer dust identified in mid-IR surveys may also be a signature of a disk in a transitional state from protoplanetary to debris disk (Meyer et al. 2007).

"Transition disks" are especially interesting as possible evolutionary links between the optically thick (Class II) disk systems and the older optically thin debris disk systems. Transition disks may be evolved protoplanetary disks with inner holes caused by clearing of the initial gas-dominated disks (Strom et al. 1989). Recent photometric work by Silverstone et al. (2006) found 5 young (<10 Myr) solar-type stars with optically thick disks out of 74 searched at mid-IR wavelengths. They note that they have not found any optically thin disks that emit in the mid-IR, indicating that their sample of excesses consists entirely of pre–main-sequence classical T Tauri objects. Megeath et al. (2005) identified 4 candidate solar and lower mass transition disks in η Cha, of the 17 stars investigated. Three of the four sources indicate accretion based on their Hα profiles. Sicilia-Aguilar et al. (2006) have also identified a number of candidate transition disks, including intermediate-mass stars that exhibit mid-IR excesses. Hernández et al. (2006) identify a B9 star that exhibits an excess at both [8.0] and [24] and has a spectral energy distribution (SED) similar to β Pictoris. Identifying and studying such a sample of mid-IR excess sources is an important step in understanding disk evolution.

In this paper we present results of a search for mid-IR excesses in the *Spitzer* Galactic Legacy Infrared Mid-Plane Survey Extraordinaire (GLIMPSE; Benjamin et al. 2003) and *MSX* catalogs to determine the fraction of mid-IR excess sources among field stellar populations. We begin with stellar sources from the Tycho-2 Spectral Catalog (Wright et al. 2003), as this is the largest available compilation of stellar classifications needed to model the SED and identify extraphotospheric emission. In § 2 we describe the sample selection and source matching between the optical and IR catalogs. We also describe new optical spectroscopy used to determine and/or confirm temperature and luminosity classifications for a small subsample of mid-IR excess sources. In § 3 we identify stars with mid-IR excesses by comparing photometric colors to model SEDs. In § 4 we confirm the mid-IR excess for some sources through 24 μm Multiband Imaging Photometer for *Spitzer* (MIPS; Rieke et al. 2004) measurements from the MIPSGAL (PID 20597) survey. For stars with mid-IR excesses and at least one measurement at $\lambda > 8$ μm, we model the excess as a single-temperature blackbody to estimate the probable disk temperatures and fractional infrared luminosities in § 5.

2. DATA

2.1. *GLIMPSE*

2.1.1. *IR Photometry*

The GLIMPSE project is one of the *Spitzer* Legacy Programs. GLIMPSE mapped the Galactic plane in four infrared array camera (IRAC; Fazio et al. 2004) bandpasses, [3.6], [4.5], [5.8], and [8.0] μm from $|l| = 10^\circ$–65° and $|b| \leq 1^\circ$ (Benjamin et al. 2003). This survey has generated a Point Source Catalog of 3×10^7 objects. To be included in the GLIMPSE Point Source Catalog, a source must have a signal-to-noise ratio greater than 5:1 with at least two detections in one band, at least one detection in an adjacent band, and flux densities greater than 0.6, 0.6, 2, and 10 mJy (in bands [3.6], [4.5], [5.8], and [8.0], respectively). See the GLIMPSE Data Products Description[15] for further documentation. Within the GLIMPSE data reduction pipeline, *JHK* photometry was performed using Two Micron All Sky Survey (2MASS) images (Cutri 2003), and sources were cross-correlated with GLIMPSE sources. The GLIMPSE program is the largest, most sensitive mid-infrared survey of the Galactic plane to date. Given the sensitivity of GLIMPSE, the survey is able to detect at 8 μm the photospheres of unreddened main-sequence A stars to $\sim$600 pc, F stars to $\sim$300 pc, G stars to $\sim$200 pc, and K stars to $\sim$140 pc. Figure 1 shows the distance at which unreddened main-sequence stars are detectable in all three catalogs used in this investigation. The solid line shows the maximum detection distance as a function of spectral type for the $V = 11.5$ (95% completeness) magnitude limit of the Tycho-2 Catalog (Hog et al. 2000) from which the Tycho-2 Spectral Catalog sources and magnitudes are drawn. The dashed line shows the maximum detection distance for GLIMPSE at [8.0]. The dotted line shows the detection limit for the *MSX* Catalog A band, which is centered at $\sim$8.28 μm. This figure shows that the vast majority of the unreddened mid-IR sources detected in GLIMPSE or *MSX* should

[15] GLIMPSE Team Web site http://www.astro.wisc.edu/sirtf/docs.html.

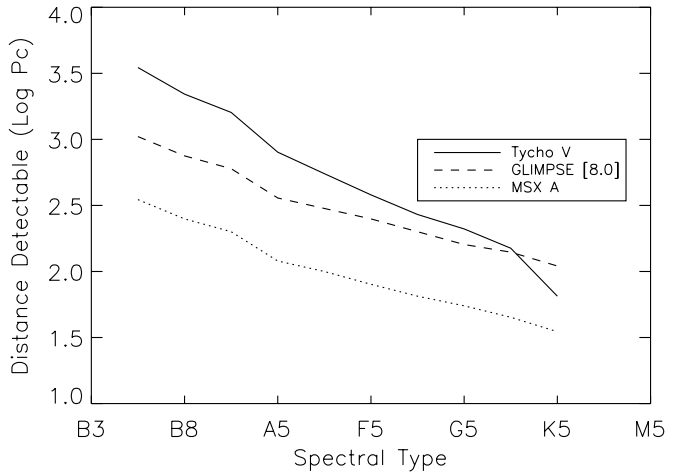

FIG. 1.—Limiting distance for main-sequence stars, as a function of spectral type, for inclusion in the Tycho-2, GLIMPSE, and *MSX* catalogs. The solid line shows the distance at which Tycho magnitudes reach $V = 11.5$, 95% completeness. The dashed line is the distance at which IRAC [8.0] reaches a flux of 10 mJy. The dotted line is the distance at which *MSX* A band reaches a flux of 100 mJy.

have optical counterparts in the Tycho-2 Catalog. Given these distances, the combined catalogs allow a survey for stars exhibiting mid-IR excesses over a much larger volume than any previous study.

Of the 4043 Tycho-2 Spectral Catalog stars within the GLIMPSE region, we matched 3361[16] with sources in the GLIMPSE Point Source Catalog (ver. 1.0) to produce a working database with *B*,[17] *V*, 2MASS *J*, *H*, *K*, and GLIMPSE [3.6], [4.5], [5.8], [8.0] photometry. The matching criteria required that the positions of GLIMPSE and Tycho-2 Spectral sources were within 3″ of each other with no additional sources inside this radius. Only 37 Tycho-2 sources had multiple GLIMPSE sources within a 3″ radius, and these were rejected. The median separation for Tycho-2 Spectral and GLIMPSE sources is 0.4″, and 99.6% of the sources were within 1″. The probability of a false match can be estimated by determining the ratio of the average source density to the area searched for an infrared counterpart to the Tycho star. However, the limiting magnitude at [3.6] is ~14 mag, while a Tycho star will be brighter than 10.5 mag at [3.6] using very conservative estimates. With 3.0×10^7 sources in the GLIMPSE Point Source Catalog over an area of 220 deg^2, there are 0.011 sources arcsec^{-2} or an average area of 91 arcsec^2 per source. If we limit the GLIMPSE catalog to sources that would be similar in brightness to Tycho sources ($[3.6] < 10.5$), we are left with 1.5×10^6 sources over a 220 deg^2 area. The source density of possible confusing sources is 5.3×10^{-4} arcsec^{-2}. Allowing a maximum separation of 1.0″ between the Tycho source and the matched GLIMPSE source, there is a 0.2% chance of positional coincidence (i.e., $\pi \times 1.0^2 \times 0.00053 = 0.002$) for GLIMPSE sources distributed randomly. Another way of stating this is that the average source separation for possible confusing GLIMPSE sources is ~24″, whereas the median separation between Tycho and GLIMPSE counterparts is 0.4″. This probability, multiplied by the number of Tycho sources (3361), predicts that, at most, seven objects could be chance matches between a Tycho star and an unrelated GLIMPSE object. One common signature of a false match or confusion with an unrelated background object would be a discontinuity in the SED between the Tycho bands and 2MASS bands, or between the 2MASS bands and the GLIMPSE bands. We found some ~30 objects where the SEDs showed such discontinuities, and these objects were discarded as unreliable matches or possibly objects with photometric variability.

Some objects lack photometry at one or more of the nine bandpasses, primarily because of saturation in GLIMPSE at magnitudes brighter than 7 at [3.6] or because of the 5 σ sensitivity limit of 10 mJy at [8.0]. Objects with no [8.0] measurement, 218 stars, were removed, leaving 3143 stars in the GLIMPSE sample. The GLIMPSE sample includes 1203 main-sequence or near–main-sequence stars with luminosity classification V, IV, or IV/V. The remainder either have no luminosity classification or are evolved stars with luminosity class I, II, or III.

2.1.2. *Optical Spectra of Selected Sources*

We obtained optical spectroscopy of a small subset of 38 stars from the GLIMPSE sample at declinations higher than −20° with the WIRO-Spec instrument on the Wyoming Infrared Observatory (WIRO) on the nights of 2005 September 17–19 using the 2400 line mm^{-1} volume-phase holographic grating. The instrument is an integral field unit spectrograph consisting of 293 densely packed fibers in a 19×20 configuration with each fiber projecting to 1″ on the sky. This grating provides a dispersion of 0.38 Å pixel^{-1}, a spectral resolution of 0.83 Å, and wavelength coverage of ~780 Å from ~4150 to 4900 Å. This wavelength regime covers hydrogen Balmer β and γ, several helium lines, and a few metal lines that are useful for luminosity and temperature classification. Standard reduction techniques were utilized, including flat-fielding using a continuum lamp and wavelength calibration using a CuAr arc lamp, but no flux calibration was performed. A typical signal-to-noise ratio of 100:1 pixel^{-1} was achieved.

We also obtained optical spectroscopy of an additional subsample of 27 stars from the GLIMPSE sample using the WIRO-Longslit spectrograph on the night of 2005 November 20. Of the 27 stars, 19 had been observed with WIRO-Spec. The WIRO-Longslit is a low-resolution spectrograph with a dispersion of 1.1 Å pixel^{-1}, a resolution of 2.6 Å using a 2″ slit width, and covering ~3800–6100 Å. The long-slit data provided more metal lines for classification and were useful for comparison with the WIRO-Spec data and spectral classifications from the literature. The same reduction procedures were performed for the long-slit data as WIRO-Spec data. A typical signal-to-noise ratio in excess of 50:1 pixel^{-1} was achieved.

Our goal was to obtain classification spectra and confirm the cataloged spectral types for a small subset of objects. This subsample covered a range of spectral and luminosity classes but preferentially consisted of B stars. Combining the higher resolution of WIRO-Spec with the greater wavelength coverage of WIRO-Longslit, we were able to modify or improve on both the temperature and luminosity classification for 12 of the 46 stars. Those 12 stars are listed in Table 1 along with our improved spectral classifications. The stars were classified by eye using comparison spectra (Yamashita et al. 1976). Two of the 12 stars in Table 1 show a significant deviation from the original classification. The first of the two sources is G010.4468+00.0629, which was classified as a B3/5 Ib in the Tycho-2 Spectral Catalog, but our spectrum lacks the C II λ4267 line that is present in supergiants. The spectrum for this source more closely resembles a B3/5 V star. The other star is G015.0981+00.3409, which was classified as a B7/8 (III), but the He I lines are similar to those of a main-sequence

[16] The Tycho sources not matched with a GLIMPSE source were, in all but the instances to be discussed below, the brightest Tycho stars that are saturated in GLIMPSE and not included in the catalog.

[17] Johnson *B* and *V* were derived from the linear transformation of Tycho B_T and V_T, $V_J = V_T - 0.090(B - V)_T$ and $(B - V)_J = 0.850(B - V)_T$; see the Tycho Catalog for descriptions.

TABLE 1
Revised Spectral/Luminosity Classes

ID (1)	Tycho Spectra (2)	WIRO Spectra (3)	Classification Basis (4)
G010.4468+00.0629	B3/5 IB	B3/5 V	No C II λ4267 but had He I λ4388
G015.0981+00.3409	B7/8 (III)	B5 Ve	Hβ absorption with emission core, weak He I λ4713
G026.7861−00.7723.....	G0	G0 I	Narrow lines
G031.3962−00.4802.....	F2/3	F2 II	Ba II λ4554 present
G036.8722−00.4112.....	B8	B8 V	Broad deep Balmer lines, Mg II λ4481 > He I λ4471
G047.3677+00.6199	B9	B8 Ve	Hβ absorption with emission core, He I λ4471 $\geq$ Mg II λ4481, He I λ4471 > He I λ4388
G047.4523+00.5132	A0	A0 V	Mg II λ4481 and Balmer series only lines present in spectral range
G051.6491−00.1182.....	A0	A0 V	Mg II λ4481 and Balmer series only lines present in spectral range
G060.5455−00.0757.....	B0 II	O9/9.5 Ib	He II λ4542 and He II λ4200 present, He II λ4686 > He I λ4716
G063.5770−00.3387.....	B9	B9 V	Mg II λ4481 > He I λ4471, broad Balmer lines
G063.6150−00.8305.....	B5	B5 Ve	Hβ absorption with emission core, He I λ4481 > Mg II λ4471
G064.3921+00.0872	B8	B8+G	Mg λ4481 $\simeq$ He λ4471, Ca λ4227 present, Fe I lines present, strong Balmer lines

Notes.—Col. (1): GLIMPSE ID. Col. (2): Tycho-2 spectral catalog classification. Col. (3): Revised classification from WIRO observations. Col. (4): Classification basis.

star. This star also has Balmer emission, and we reclassified it as a B5 Ve star. Most stellar classifications were consistent within two temperature subclasses. Since less than 5% of the sample, 2 of 46, have a significant change in spectral type, we assume that the majority of the literature classifications from the Tycho-2 Spectral Catalog are approximately correct and use them for analysis.

2.2. *MSX*

MSX surveyed the entire Galactic plane within $b = \pm 5^{\circ}$, and it covered additional regions including the Large and Small Magellanic Clouds in six bands: 4.29 (B1), 4.35 (B2), 8.28 (A), 12.13 (C), 14.65 (D), and 21.34 μm (E) (Price et al. 2001). The *MSX* survey was less sensitive than GLIMPSE, having greatest sensitivity at 8.28 μm (0.1 Jy; Egan et al. 2003), corresponding to 200 pc for unreddened main-sequence A stars, 100 pc for F stars, 65 pc for G stars, and 45 pc for K stars. We matched 8688 Tycho-2 Spectral Catalog sources to *MSX* catalog positions. The matching criteria required that the positions of the *MSX* and Tycho-2 Spectral sources were within 6″ with no additional sources inside this radius; the beam size at 8 μm is 5″. The median separation for Tycho-2 Spectral and *MSX* sources is 0.8″ with 68.8% of matches within 1″. The 1 σ positional accuracy of *MSX* is 2″ (Egan et al. 2003). We then matched the 8688 *MSX* and Tycho-2 Spectral sources to the nearest 2MASS source requiring that the 2MASS source is within 1″ of the Tycho-2 Spectral source position. The probability of a false match can be estimated by determining the ratio of the average source density to the area searched for an infrared counterpart to the Tycho star. The *MSX* Catalog has $\frac{1}{7}$ the number of sources as the GLIMPSE Catalog. As a (very) conservative estimate, we use the GLIMPSE source density of 0.00054 sources arcsec^{-2} when determining probability of a chance coincidence. The actual *MSX* source density is approximately a factor of 10 lower. Using twice the median separation of sources, 1.6″ as a realistic average separation, yields a probability of a random positional coincidence of 0.4% (e.g., $\pi \times 1.6^2 \times 0.00054 = 0.004$).

3. IDENTIFYING THE EXCESS

The goal of our analysis is to identify stars with mid-IR excesses in the GLIMPSE and *MSX* samples for the purpose of finding stars with circumstellar disks. We expect circumstellar disks to exist primarily around main-sequence stars or proto-stars. Evolved stars may exhibit IR excesses owing to dust in cool extended atmospheres or thermal bremsstrahlung emission (Barlow & Cohen 1977). Therefore, we separate the GLIMPSE sample into main-sequence or near–main-sequence objects (luminosity class IV or V) and evolved stars (luminosity classes I, II, III). Main-sequence O and early B stars often produce localized H II regions with thermal bremsstrahlung components that may contribute to an extraphotospheric excess at IR wavelengths (e.g., Gehrz et al. 1974). In § 3.3 we discuss in more detail the signatures of thermal bremsstrahlung emission in the SEDs. We further separate main-sequence stars into those earlier than B8 and those B8 or later. In the GLIMPSE main-sequence sample there are 253 B stars (B8 or later), 391 A stars, 247 F stars, 109 G stars, and 24 K stars of luminosity class V, IV, or IV/V. For the *MSX* sample we removed all luminosity class I, II, III and unknown objects, leaving 872 main-sequence and near–main-sequence stars (luminosity class V, IV, or IV/V). We do not tabulate evolved stars in the *MSX* sample because of the large number of such objects and the limited interest in mid-IR excesses among this population. See Clarke et al. (2005) for a tabulation of such objects. We further separate the *MSX* main-sequence stars into those earlier than B8 and those B8 or later. The *MSX* main-sequence sample consists of 45 B stars (B8 or later), 118 A stars, 238 F stars, 233 G stars, and 151 K stars.

3.1. *GLIMPSE*

The photometric data for each object in the entire GLIMPSE subsample of 3143 stars were fitted with Kurucz ATLAS9 models using temperatures and effective gravities corresponding to the nearest spectral type (Kurucz 1993). This method is similar to that used by Uzpen et al. (2005) to identify excess sources in the field of RCW 49. We calculated $K - [8.0]$ color excesses, $E(K - [8.0])$, by measuring the differences between the Kurucz photospheric model and the photometric $K - [8.0]$. The Kurucz photospheric model colors were determined by passing the stellar model through digitized transmission curves of the selected bandpasses. We chose the $K - [8.0]$ color because main-sequence stars should exhibit minimal color for these wavelengths since both bandpasses are on the Rayleigh-Jeans tail of the stellar blackbody spectrum. This method is similar to that employed by Aumann & Probst (1991), who used $K - [12]$ to identify warm disk candidates.

We required that the "excess" stars have an $E(K - [8.0])/\sigma_{(K-[8.0])} \geq 3$, where $\sigma_{(K-[8.0])} = (\sigma_K^2 + \sigma_{[8.0]}^2 + \sigma_{\rm cal}^2)^{1/2}$.

Included in this uncertainty is a 5% absolute calibration uncertainty, $\sigma_{\rm cal}$, for IRAC (Reach et al. 2005). Among the 3143 GLIMPSE stars we find 167 objects with mid-IR excesses. Table 2 gives the spectral types, magnitudes, and uncertainties for the 20 luminosity class IV or V stars and eight unknown luminosity class objects B8 or later that met the above criteria. Table 3 contains spectral types, magnitudes, and uncertainties for 139 stars earlier than B8 and post–main-sequence stars.

Figure 2 shows a histogram of $E(K - [8.0])$ for both the 167 excess sources (*dotted line*) and 2919 nonexcess sources (*solid line*), demonstrating that the excess sources form a positive tail to the distribution. Photometric uncertainties cause some overlap between the excess and nonexcess sources. Stars with genuine excesses can have small $E(K - [8.0])$ as long as the photometric uncertainties are small. This population of objects will overlap in Figure 2 with nonexcess objects that have large $E(K - [8.0])$ but large uncertainties. For example, the nonexcess star G035.1185−00.7465 has $E(K - [8.0]) = 0.48$ and $\sigma_{(K-[8.0])} = 0.19$, while the excess star G014.4239−00.7657 also has $E(K - [8.0]) = 0.48$ and $\sigma_{(K-[8.0])} = 0.12$. Figure 3 shows a histogram of $E(K - [8.0])/\sigma_{(K-[8.0])}$, revealing a large population of stars that have $E(K - [8.0])/\sigma_{(K-[8.0])} \geq 3$. Some sources also appear to have $E(K - [8.0])$ deficits. There are only 10 sources with a deficit $E(K - [8.0])/\sigma_{(K-[8.0])} \leq -3$. In these sources the [8.0] measurement lies below the best-fitting photospheric model. The occurrence of $E(K - [8.0])$ deficits less than 3 σ is $\sim$0.3%, consistent with the expected fraction exceeding 3 σ from a normal distribution. Conversely, we would also expect 10 stars, 6% of our 167-star excess sample, to exhibit a false [8.0] excess on statistical grounds. We discuss the removal of these false excess sources in § 4. M stars (27 objects) that are poorly fitted by Kurucz models and stars that show zero-point photometric offsets between IRAC and 2MASS ($\sim$30 objects), possibly due to variability, were omitted from Figures 2 and 3. Figure 4 shows the distribution among spectral types for the 50 main-sequence excess objects (*dotted line*) and 1153 nonexcess objects (*solid line*). The distribution of nonexcess objects is broad and peaks near A0, while virtually all of the excess sources are earlier than A5. A two-sided K-S test on the distributions of excess and nonexcess spectral types shows that there is less than a 10^{-8} probability of obtaining the excess distribution from the nonexcess population. Therefore, the population exhibiting mid-IR excesses preferentially consists of late B and early A stars, as would be expected for systems capable of producing hot dust excesses. The spectral type distribution of excess stars is inconsistent with being drawn at random from among the Tycho-2 Spectral Catalog parent population, as should be expected if the excesses were caused by confusion with unrelated background objects.

3.2. *MSX*

We fit the *MSX* sample stars with a Kurucz model in the same manner as the GLIMPSE sample. We used the same reliability constraints on the *MSX* sources, $E(K - [8.0])/\sigma_{(K-[8.0])} \geq 3$, and include an absolute photometric uncertainty in $\sigma_{K-[8.0]}$ of 5% (Price et al. 2001). There are 63 stars that exhibit a photometric excess of $E(K - [8.0])/\sigma_{(K-[8.0])} \geq 3$ in the *MSX* sample. The 19 stars of spectral type B8 or later are listed in Table 4, while the 44 stars earlier than B8 are listed in Table 5.

Figure 5 is a histogram of $E(K - [8.0])$ for the main-sequence *MSX* sources. Objects identified as having an excess (*dotted line*) form a positive tail to the distribution of nonexcess sources (*solid line*). The two histograms overlap slightly for the same reason as the overlap in Figure 2. The *MSX* sample peaks at $E(K - [8.0]) = -0.12$, implying that a small systematic calibration uncertainty may be present given that normal stars should have zero color.[18] Since the median $E(K - [8.0])$ is negative, the stars with the largest deficits, eight sources, have $E(K - [8.0]) < -0.4$. Two of the eight sources have an $E(K - [8.0])$ deficit but a C-band excess, implying a possible contribution from a structured background. One of the eight sources is an M star and is poorly fitted by the Kurucz models. The remaining deficit sources have only an A-band measurement and deficit. Given that the fractional occurrence for the deficit sources is less than 1% and for excess sources is over 4%, we include all excess sources but note that some excess sources may be spurious. Figure 6 shows the distribution of spectral types in the *MSX* sample. The distribution peaks among late-type stars, as is expected given the nature of the stellar initial mass function and the biases of a magnitude-limited survey. The *MSX* sample shows excesses among all spectral types and has proportionally more late-type excess sources than the GLIMPSE sample. We speculate that GLIMPSE contains proportionally more early-type stars as a result of saturation in the IRAC bands. The IRAC [8.0] saturates at $\simeq$0.7 Jy in GLIMPSE exposure times. For a 5500 K blackbody, stars brighter than $V \simeq 7$ will saturate, and for a 10,000 K blackbody, stars brighter than $V \simeq 5$ will saturate. Thus, late-type stars are preferentially missing from GLIMPSE compared to early-type stars. The distribution of spectral types in the *MSX* sample (Fig. 6) essentially confirms this hypothesis, given that virtually all of the *MSX* stars would be saturated in GLIMPSE.

3.3. *The Mid-IR Excesses*

The origin of the mid-IR excesses may be something other than absorption and reemission of photospheric energy by small dust particles in a circumstellar disk. One alternative process could be thermal bremsstrahlung emission, most likely to arise among the early O and B stars and supergiants listed in Table 3. To test whether free-free emission could be a viable explanation for the excess, an optically thin, thermal bremsstrahlung component was included without a blackbody disk component in the modeling of the stars' SEDs. The normalization of the bremsstrahlung component is a free parameter along with extinction and distance. Models with bremsstrahlung components fit the SEDs of O and early B stars, which typically have all four IRAC bands in excess of the model photosphere, better than the models with a single blackbody component. An example of an SED with the thermal bremsstrahlung component is shown in Figure 7. A blackbody component with a single temperature provides a poor fit to the four IRAC measurements in excess of the photosphere. Since early-type stars are ionizing stars and they can be fitted better by photospheric plus thermal bremsstrahlung models, free-free emission becomes an increasingly likely explanation for the mid-IR excess of stars earlier than B8. We use B8 or later as our cutoff for systems with excesses plausibly explained by circumstellar disks.

IR excesses may instead be caused by diffuse interstellar emission or multiple confusing sources in the telescope beam rather than any form of circumstellar disk. A few examples of previously identified excess sources from *IRAS* with interstellar rather than circumstellar dust origins are found in Kalas et al. (2002). However, given that the angular resolution of IRAC at [8.0] is approximately 10 times better than *IRAS* at 12 μm, the probability of spurious excesses from unrelated sources in the beam is greatly reduced. Without additional measurements, either spectroscopic or coronagraphic, this possibility cannot entirely be

[18] For the *MSX* band A we use a photometric zero point of 58.49 Jy from Cohen et al. (2000).

TABLE 2

PHOTOMETRIC PARAMETERS FOR MAIN-SEQUENCE STARS B8 OR LATER WITH MID-IR EXCESSES FROM GLIMPSE

Table (1)	ID (2)	Spectral Type (3)	V (mag) (4)	B (mag) (5)	J (mag) (6)	$[J]\sigma$ (mag) (7)	H (mag) (8)	$[H]\sigma$ (mag) (9)	K (mag) (10)	$[K]\sigma$ (mag) (11)	[3.6] (mag) (12)	σ[3.6] (mag) (13)	[4.5] (mag) (14)	σ[4.5] (mag) (15)	[5.8] (mag) (16)	σ[5.8] (mag) (17)	[8.0] (mag) (18)	σ[8.0] (mag) (19)
1.....	G011.2691+00.4208	B9 V	8.29	8.38	7.88	0.02	7.90	0.05	7.82	0.03	7.64	0.04	7.74	0.04	7.68	0.04	7.48	0.05
2.....	G014.4239−00.7657	B8	10.94	10.92	10.32	0.03	10.29	0.03	10.24	0.03	10.23	0.07	10.11	0.05	10.16	0.09	9.77	0.10
3.....	G027.0268+00.7224	A0 V	9.47	9.81	8.01	0.02	7.59	0.04	7.41	0.02	7.31	0.04	7.27	0.04	7.28	0.05	7.07	0.03
4.....	G036.8722−00.4112	B8 V	8.69	8.95	7.94	0.02	7.88	0.03	7.82	0.02	7.72	0.06	7.67	0.06	7.65	0.04	7.55	0.03
5.....	G042.9876+00.4201	B8 V	9.00	9.30	8.24	0.02	8.19	0.02	8.14	0.02	7.86	0.05	7.80	0.06	7.75	0.04	7.59	0.04
6.....	G047.3677+00.6199	B8 Ve	7.93	7.98	7.71	0.03	7.69	0.05	7.68	0.02	7.45	0.04	7.25	0.03	7.11	0.04	6.75	0.02
7.....	G047.4523+00.5132	A0 V	9.74	9.94	9.00	0.03	8.93	0.03	8.85	0.02	8.76	0.05	8.84	0.06	8.84	0.04	8.56	0.03
8.....	G051.6491−00.1182	A0 V	8.11	8.17	7.80	0.03	7.84	0.05	7.82	0.03	7.81	0.04	7.78	0.06	7.82	0.04	7.63	0.03
9.....	G060.2596−00.5188	B 8 V	9.22	9.24	9.03	0.03	9.03	0.03	9.05	0.02	9.07	0.05	9.05	0.07	9.05	0.06	8.30	0.08
10.....	G063.5770−00.3387	B9 V	9.76	9.99	9.05	0.02	9.03	0.02	8.98	0.02	8.95	0.04	...	...	8.98	0.05	8.63	0.04
11.....	G064.3921+00.0872	B8+G	10.18	10.56	9.06	0.03	8.97	0.02	8.81	0.02	8.73	0.04	8.72	0.05	8.72	0.04	8.48	0.03
12.....	G299.1677−00.3922	B8	9.31	9.41	9.14	0.02	9.10	0.03	9.05	0.03	9.05	0.05	8.99	0.06	8.90	0.05	8.70	0.04
13.....	G299.7090−00.9704	B8/9 IV	9.35	9.50	8.94	0.02	8.92	0.02	8.86	0.02	8.83	0.05	8.79	0.05	8.77	0.05	8.68	0.04
14.....	G300.0992−00.0627	A1	10.07	10.23	9.57	0.03	9.44	0.03	9.40	0.03	9.29	0.04	9.19	0.06	9.04	0.05	8.84	0.03
15.....	G305.1140−00.2353	B8/9 V	9.90	10.17	9.12	0.03	9.01	0.02	8.96	0.02	8.82	0.05	8.86	0.03	8.85	0.04	8.75	0.03
16.....	G305.4232−00.8229	B6/8 V(E)	9.28	9.40	8.77	0.03	8.73	0.03	8.64	0.02	8.46	0.04	8.32	0.05	8.16	0.05	7.85	0.03
17.....	G307.9784−00.7148	B8 V(N)	7.93	7.92	7.83	0.03	7.81	0.04	7.76	0.03	7.61	0.04	7.74	0.06	7.57	0.02	7.36	0.04
18.....	G309.4316−00.3222	B8 V	9.87	9.89	9.69	0.02	9.63	0.03	9.59	0.03	9.43	0.05	9.50	0.05	9.37	0.05	9.33	0.05
19.....	G310.5420+00.4120	B8 IV(N)	9.03	9.08	8.76	0.02	8.77	0.04	8.71	0.02	8.68	0.03	8.81	0.06	8.72	0.04	8.46	0.04
20.....	G311.0099+00.4156	A3 IV	8.12	8.34	7.56	0.02	7.48	0.03	7.36	0.02	7.24	0.05	7.22	0.05	7.33	0.05	6.99	0.07
21.....	G311.6185+00.2469	B8/9 IV/V	9.88	9.99	9.48	0.02	9.45	0.02	9.40	0.02	9.32	0.04	9.33	0.06	9.34	0.05	9.12	0.05
22.....	G314.3136−00.6977	A1 IV	8.53	8.66	8.01	0.02	7.96	0.03	7.91	0.02	7.84	0.04	8.01	0.05	7.83	0.03	7.69	0.03
23.....	G320.1546−00.7551	B9.5 IV/V	9.93	10.05	9.45	0.02	9.41	0.02	9.39	0.02	9.29	0.04	9.43	0.05	9.27	0.04	9.11	0.06
24.....	G321.7868+00.4102	B8 VN	9.16	9.20	9.01	0.02	8.97	0.03	8.90	0.02	8.75	0.04	8.72	0.05	8.50	0.03	8.13	0.04
25.....	G322.6930+00.0572	F7/G0	10.28	10.97	9.08	0.02	8.78	0.05	8.68	0.02	8.29	0.04	8.31	0.05	8.32	0.05	8.23	0.03
26.....	G339.4392−00.7791	A0/1 IV/V	9.61	9.82	8.53	0.02	8.23	0.06	8.07	0.02	7.89	0.06	7.95	0.06	7.82	0.05	7.73	0.02
27.....	G339.7415−00.1904	A0	10.48	10.48	10.01	0.03	9.99	0.03	10.00	0.04	9.98	0.05	9.93	0.05	10.02	0.07	9.73	0.06
28.....	G340.0517+00.6687	B8	9.59	9.88	8.39	0.03	8.24	0.04	8.04	0.02	7.64	0.04	7.52	0.05	7.30	0.05	6.93	0.03

NOTES.—Col. (1): Table number. Col. (2): GLIMPSE ID number. Col. (3): Spectral type from Tycho-2 Spectral Catalog. Col. (4): V magnitude. Col. (5): B magnitude. Col. (6): 2MASS J magnitude. Col. (7): 1 σ uncertainty for J. Col. (8): 2MASS H magnitude. Col. (9): 1 σ uncertainty for H. Col. (10): 2MASS K magnitude. Col. (11): 1 σ uncertainty for K. Col. (12): [3.6] magnitude. Col. (13): 1 σ uncertainty for [3.6]. Col. (14): [4.5] magnitude. Col. (15): 1 σ uncertainty for [4.5]. Col. (16): [5.8] magnitude. Col. (17): 1 σ uncertainty for [5.8]. Col. (18): [8.0] magnitude. Col. (19): 1 σ uncertainty for [8.0].

TABLE 3

PHOTOMETRIC PARAMETERS FOR MAIN-SEQUENCE STARS EARLIER THAN B8 AND POST–MAIN-SEQUENCE STARS WITH MID-IR EXCESSES IN GLIMPSE

Table (1)	ID (2)	Spectral Type (3)	V (mag) (4)	B (mag) (5)	J (mag) (6)	$[J]\sigma$ (mag) (7)	H (mag) (8)	$[H]\sigma$ (mag) (9)	K (mag) (10)	$[K]\sigma$ (mag) (11)	[3.6] (mag) (12)	σ[3.6] (mag) (13)	[4.5] (mag) (14)	σ[4.5] (mag) (15)	[5.8] (mag) (16)	σ[5.8] (mag) (17)	[8.0] (mag) (18)	σ[8.0] (mag) (19)
1.....	G010.0898+00.5289	B1/2 (I)N	8.49	8.87	7.02	0.02	6.78	0.05	6.48	0.02	[a]	...	[a]	...	5.18	0.04	4.83	0.02
2.....	G010.4468+00.0629	B3/5 V	8.40	8.67	7.45	0.02	7.28	0.04	7.09	0.02	[a]	...	[a]	...	6.26	0.04	5.98	0.02
3.....	G010.6669−00.0339	B5 II	9.15	9.44	7.89	0.02	7.76	0.05	7.58	0.02	7.26	0.04	7.11	0.06	6.86	0.04	6.64	0.03
4.....	G011.1473+00.2092	B9 IB/II	9.59	9.76	8.92	0.02	8.88	0.04	8.81	0.02	8.66	0.03	8.77	0.05	8.78	0.04	8.55	0.03
5.....	G011.7709−00.9755	B5 III/V	9.19	9.35	8.58	0.02	...	...	8.49	0.03	8.49	0.06	8.57	0.06	8.41	0.05	8.29	0.03
6.....	G011.7928+00.6478	B7/8 IB	10.14	10.30	9.34	0.02	9.26	0.02	9.21	0.02	8.98	0.05	9.01	0.07	9.10	0.05	8.84	0.04
7.....	G012.1238+00.4899	B3 (II)E	9.01	9.29	7.68	0.02	7.52	0.05	7.28	0.03	[a]	...	6.74	0.06	6.51	0.04	6.26	0.03
8.....	G012.1292+00.0934	B0?VPE	10.12	10.32	8.49	0.02	8.16	0.04	7.91	0.03	7.52	0.06	7.38	0.05	7.29	0.04	7.03	0.03
9.....	G012.2041−00.0783	B8 II	8.20	8.23	7.92	0.02	7.89	0.04	7.43	0.02	[a]	...	[a]	...	4.87	0.05	4.26	0.04
10.....	G013.1871−00.6730	B3/5 III	9.63	9.80	9.22	0.03	9.16	0.02	9.09	0.02	9.03	0.03	9.09	0.06	9.09	0.05	8.85	0.04
11.....	G013.6264−00.3992	B9 III	9.28	9.38	8.72	0.03	8.50	0.03	7.86	0.03	[a]	...	6.66	0.10	6.61	0.04	6.69	0.05
12.....	G014.7861−00.4436	B8 III	8.75	8.90	8.17	0.03	8.15	0.05	8.11	0.02	8.04	0.04	8.01	0.05	8.01	0.05	7.94	0.03
13.....	G014.8385+00.2174	B3 II	10.08	10.30	9.38	0.02	9.27	0.03	9.21	0.03	9.08	0.04	9.02	0.05	8.83	0.04	8.65	0.03
14.....	G014.8421+00.8391	B8 IB/II	10.62	10.79	9.76	0.03	9.61	0.02	9.49	0.02	9.32	0.06	9.21	0.05	9.04	0.04	8.71	0.04
15.....	G015.0981+00.3409	B5 Ve	9.57	9.85	8.58	0.02	8.50	0.04	8.50	0.02	8.33	0.05	8.22	0.06	8.33	0.05	8.17	0.03
16.....	G016.8760+00.6456	B1:V:NE	9.99	10.42	8.73	0.03	8.43	0.04	8.10	0.02	7.03	0.05	6.74	0.10	6.59	0.03	6.28	0.03
17.....	G016.9372+00.8375	O5	8.32	8.69	6.89	0.02	6.69	0.03	6.57	0.02	[a]	...	[a]	...	6.12	0.04	5.93	0.03
18.....	G016.9776+00.8159	B0 IV	10.30	10.55	8.25	0.02	8.08	0.05	7.94	0.03	7.88	0.04	7.91	0.06	7.88	0.05	7.64	0.05
19.....	G017.8424−00.1736	B9.5 III	9.81	10.18	8.46	0.03	8.37	0.04	8.27	0.03	8.05	0.06	[a]	...	8.11	0.05	8.02	0.04
20.....	G017.9884−00.8228	B8 IA	9.48	10.16	7.50	0.02	7.27	0.03	7.14	0.02	[a]	...	6.87	0.05	6.94	0.03	6.80	0.03
21.....	G018.5200+00.8376	B	10.34	11.42	6.74	0.02	6.27	0.03	6.02	0.02	[a]	...	[a]	...	5.69	0.03	5.55	0.02
22.....	G018.9608+00.3773	B1,5 IA	8.95	9.99	5.77	0.02	5.38	0.02	5.08	0.02	[a]	...	[a]	...	4.70	0.04	4.58	0.02
23.....	G019.1678+00.3235	O6:	11.22	12.60	7.82	0.03	7.43	0.02	7.22	0.02	7.04	0.04	6.95	0.04	6.95	0.04	6.83	0.03
24.....	G020.0232+00.2388	B0.5 II/I	8.65	9.50	6.11	0.05	5.81	0.04	5.65	0.03	[a]	...	[a]	...	5.42	0.03	5.29	0.03
25.....	G023.7311−00.5366	B	11.20	11.92	8.88	0.02	8.60	0.02	8.27	0.02	7.77	0.05	7.64	0.07	7.46	0.04	7.05	0.03
26.....	G023.7912+00.0636	O9?V?P	9.60	10.42	7.46	0.03	7.19	0.03	7.03	0.02	[a]	...	6.94	0.03	6.92	0.05	6.83	0.02
27.....	G024.5309−00.8466	O6/7	9.64	10.06	8.03	0.02	7.92	0.03	7.84	0.02	7.72	0.04	7.72	0.06	7.65	0.05	7.59	0.03
28.....	G025.1974−00.8095	B1 Ib/II	9.60	9.99	8.58	0.02	8.55	0.04	8.42	0.02	8.34	0.03	8.30	0.04	8.42	0.04	8.25	0.02
29.....	G026.7861−00.7723	G0 I	9.98	11.25	7.17	0.02	6.68	0.03	6.46	0.03	[a]	...	[a]	...	6.11	0.04	6.04	0.03
30.....	G028.1595−00.7732	B0/1 Iab	8.39	9.05	6.56	0.02	6.38	0.03	6.23	0.02	[a]	...	[a]	...	6.14	0.04	6.03	0.03
31.....	G030.4620+00.3924	O9.5 III	11.39	11.89	9.19	0.02	8.91	0.03	8.80	0.03	8.63	0.06	8.58	0.06	8.70	0.05	8.56	0.04
32.....	G032.6777−00.7327	O8	10.18	10.52	8.68	0.02	8.59	0.05	8.45	0.02	8.39	0.04	8.43	0.06	8.43	0.04	8.23	0.02
33.....	G033.1638+00.8287	Nova	11.74	11.65	11.70	0.03	11.51	0.03	11.35	0.03	10.19	0.14	10.63	0.09	10.50	0.09	10.51	0.08
34.....	G044.3388−00.7118	B3P	8.02	8.16	7.56	0.02	7.57	0.03	7.48	0.02	7.56	0.04	7.51	0.03	7.40	0.04	7.24	0.03
35.....	G058.7277−00.4505	B2 V:NNE	10.08	10.40	8.90	0.02	8.78	0.02	8.49	0.02	7.90	0.04	7.82	0.06	7.54	0.04	7.16	0.03
36.....	G060.2169−00.2707	B8P	7.23	8.01	5.50	0.31	...	...	4.62	0.02	[a]	...	[a]	...	4.36	0.04	4.28	0.02
37.....	G060.5455−00.0757	O9/9.5 Ib	9.02	9.52	7.46	0.02	7.36	0.02	7.29	0.02	7.16	0.03	7.22	0.04	7.18	0.02	7.15	0.02
38.....	G061.1877−00.1385	O6F	9.30	9.85	7.59	0.02	7.41	0.04	7.32	0.02	7.25	0.05	7.24	0.07	7.24	0.05	7.16	0.03
39.....	G061.2722+00.2692	O8F	9.81	10.83	6.93	0.04	6.61	0.06	6.43	0.02	[a]	...	[a]	...	6.23	0.04	6.09	0.03
40.....	G063.6068+00.2500	A0 IB–II	10.20	10.69	8.72	0.02	8.56	0.02	8.43	0.02	8.20	0.04	8.17	0.04	8.06	0.05	7.78	0.03
41.....	G063.6150−00.8305	B5 Ve	8.73	8.99	7.76	0.02	7.72	0.07	7.54	0.02	7.35	0.05	7.21	0.05	7.07	0.03	6.66	0.02
42.....	G295.2144−00.6601	B1 IB	9.56	9.69	9.64	0.02	9.65	0.02	9.65	0.02	9.62	0.04	9.72	0.05	9.65	0.05	9.59	0.06
43.....	G295.2186−00.6598	B2 III/V	9.00	8.89	9.01	0.04	9.08	0.02	9.09	0.02	9.11	0.04	9.09	0.09	9.04	0.04	8.92	0.05
44.....	G295.2330−00.0512	B3/7	9.63	9.72	9.55	0.02	9.56	0.02	9.56	0.02	9.56	0.05	9.48	0.04	9.50	0.05	9.30	0.03
45.....	G295.4204−00.1574	B0 III	7.61	7.59	7.54	0.02	7.54	0.03	7.57	0.02	7.53	0.05	7.55	0.04	7.50	0.04	7.48	0.02
46.....	G295.6111−00.2403	O/BNE	8.97	9.15	8.68	0.03	8.58	0.06	8.40	0.03	8.07	0.03	8.01	0.06	7.82	0.03	7.69	0.03
47.....	G295.8919+00.1997	B5/7 IA/A	6.61	6.82	5.73	0.02	5.66	0.03	5.54	0.02	[a]	...	[a]	...	5.43	0.04	5.34	0.03

TABLE 3—*Continued*

Table (1)	ID (2)	Spectral Type (3)	V (mag) (4)	B (mag) (5)	J (mag) (6)	$[J]\sigma$ (mag) (7)	H (mag) (8)	$[H]\sigma$ (mag) (9)	K (mag) (10)	$[K]\sigma$ (mag) (11)	[3.6] (mag) (12)	σ[3.6] (mag) (13)	[4.5] (mag) (14)	σ[4.5] (mag) (15)	[5.8] (mag) (16)	σ[5.8] (mag) (17)	[8.0] (mag) (18)	σ[8.0] (mag) (19)
48.....	G295.9926−00.6022	A2 IAB	5.75	5.95	[a]	...	4.92	0.04	4.76	0.02	[a]	...	[a]	...	4.53	0.03	4.48	0.03
49.....	G297.0348−00.5563	A8 II	6.42	6.69	5.45	0.02	5.34	0.03	5.23	0.02	[a]	...	[a]	...	5.18	0.04	5.08	0.03
50.....	G297.1058+00.8642	B3/5(E)	9.54	9.57	9.14	0.02	9.06	0.03	8.90	0.02	8.32	0.04	8.24	0.04	8.07	0.04	7.74	0.03
51.....	G297.4025−00.3217	B1 V	8.09	8.09	7.89	0.03	7.91	0.03	7.79	0.02	7.80	0.04	7.65	0.07	7.57	0.03	7.29	0.03
52.....	G297.5561+00.3365	WR	10.63	10.77	10.20	0.02	10.08	0.02	9.83	0.02	9.53	0.05	9.25	0.06	9.05	0.06	8.61	0.04
53.....	G297.6275−00.5155	B0/1 I/II	8.82	9.12	7.60	0.03	7.45	0.05	7.35	0.02	7.28	0.05	7.26	0.05	7.13	0.03	7.09	0.06
54.....	G298.5069−00.4152	B8 IA/AB	5.99	6.22	...	...	5.04	0.03	4.93	0.02	[a]	...	[a]	...	4.77	0.04	4.62	0.03
55.....	G298.5995+00.6590	B2 IA/AB	8.82	9.44	6.82	0.02	6.52	0.02	6.37	0.02	[a]	...	[a]	...	6.13	0.04	6.00	0.02
56.....	G299.4413+00.3860	G2 IB	6.76	7.64	4.93	0.02	...	...	4.44	0.02	[a]	...	[a]	...	4.24	0.03	4.16	0.03
57.....	G299.9647+00.4753	O9.5/B0	8.79	9.09	7.69	0.03	7.63	0.05	7.50	0.02	7.41	0.05	7.41	0.04	7.44	0.03	7.28	0.03
58.....	G300.2439+00.8987	B2 IV NE	9.39	9.60	8.90	0.03	8.86	0.03	8.78	0.02	8.28	0.06	8.23	0.06	8.04	0.03	7.88	0.03
59.....	G300.4886+00.2894	O7	10.69	11.11	8.74	0.03	8.55	0.03	8.43	0.02	8.26	0.04	8.30	0.05	8.28	0.04	8.23	0.03
60.....	G300.9119−00.7057	K0	9.87	11.10	6.92	0.03	6.35	0.04	6.13	0.02	[a]	...	[a]	...	5.82	0.04	5.77	0.03
61.....	G302.0998+00.3700	B8/9 (III	9.93	10.19	8.96	0.03	8.83	0.04	8.77	0.02	8.70	0.04	8.65	0.06	8.58	0.03	8.29	0.03
62.....	G302.4708+00.3243	B7 III/V	9.88	10.16	8.79	0.03	8.73	0.04	8.59	0.02	8.48	0.04	8.41	0.03	8.35	0.03	8.05	0.02
63.....	G302.5242−00.1270	B1/3 (I)	9.45	10.02	7.51	0.03	7.21	0.03	6.92	0.02	[a]	...	[a]	...	6.14	0.03	5.85	0.03
64.....	G303.7737−00.7813	B7/8 III	8.15	8.29	7.61	0.03	7.59	0.03	7.56	0.03	7.36	0.05	7.26	0.05	7.24	0.05	7.14	0.02
65.....	G304.4853+00.9417	B2 V	10.64	10.97	9.64	0.02	9.54	0.02	9.54	0.02	9.45	0.06	9.46	0.05	9.45	0.06	9.12	0.07
66.....	G304.6239+00.5869	B2/3NE	9.84	10.01	8.94	0.02	8.76	0.05	8.61	0.02	8.22	0.04	8.05	0.05	7.88	0.03	7.47	0.03
67.....	G304.9962−00.0719	B0 III	8.76	9.20	7.22	0.03	7.07	0.04	6.98	0.02	[a]	...	6.85	0.10	6.88	0.04	6.72	0.03
68.....	G304.9962−00.0719	B0 III	8.76	9.20	7.22	0.03	7.07	0.04	6.98	0.02	[a]	...	6.85	0.10	6.88	0.04	6.72	0.03
69.....	G305.6937+00.5947	B5/7 (V)	10.13	10.19	9.69	0.02	9.67	0.02	9.59	0.02	9.60	0.04	9.59	0.04	9.49	0.04	9.24	0.03
70.....	G305.8649+00.9680	BE	9.93	10.18	8.69	0.02	8.43	0.04	8.12	0.02	7.70	0.05	7.47	0.06	7.13	0.04	6.75	0.04
71.....	G306.0516+00.5885	B3/5 III/	9.90	9.93	9.70	0.02	9.72	0.02	9.70	0.02	9.67	0.03	9.75	0.05	9.74	0.04	9.54	0.04
72.....	G306.0614+00.2154	O8	8.03	8.17	7.47	0.03	7.46	0.03	7.44	0.02	7.34	0.02	7.35	0.03	7.32	0.02	7.15	0.02
73.....	G306.1872−00.7247	B2/4 III/	9.40	9.60	8.08	0.03	7.92	0.05	7.67	0.02	7.18	0.04	7.07	0.04	6.76	0.04	6.51	0.04
74.....	G306.3011+00.6772	B0.5 IAB	8.23	8.59	6.99	0.03	6.85	0.03	6.73	0.02	[a]	...	6.76	0.06	6.65	0.05	6.50	0.04
75.....	G306.5048−00.4096	O9/B0 (V)	9.27	9.26	9.10	0.02	9.10	0.03	9.14	0.02	9.15	0.05	9.16	0.04	9.18	0.05	8.98	0.03
76.....	G306.5768+00.2057	B1 IA	10.26	10.95	8.08	0.02	7.80	0.03	7.64	0.02	7.47	0.04	7.48	0.04	7.42	0.03	7.32	0.02
77.....	G307.0512−00.0654	O9/B1 (I)	7.67	7.74	7.22	0.02	6.99	0.04	6.72	0.03	[a]	...	[a]	...	5.68	0.03	5.37	0.02
78.....	G307.1450+00.4571	B2/5 (VN)	9.56	9.64	9.28	0.02	9.26	0.02	9.21	0.02	9.13	0.04	9.14	0.06	8.99	0.05	8.87	0.04
79.....	G307.3751+00.1215	B0/1 (III	9.51	9.61	9.20	0.02	9.19	0.02	9.18	0.02	9.23	0.04	9.34	0.06	9.23	0.04	9.07	0.05
80.....	G307.5174−00.5324	B0/1 (III	7.50	7.53	7.29	0.03	7.30	0.05	7.25	0.02	7.21	0.03	7.32	0.03	7.24	0.03	7.17	0.02
81.....	G307.5320+00.4378	WC	10.73	11.15	8.74	0.03	7.91	0.03	6.84	0.03	[a]	...	[a]	...	4.96	0.02	4.62	0.03
82.....	G307.5734+00.7625	B8 III	10.00	10.02	9.57	0.03	9.48	0.03	9.32	0.02	9.15	0.04	9.10	0.06	8.77	0.04	8.40	0.03
83.....	G307.7959+00.1568	WN	10.50	10.86	8.77	0.03	8.49	0.06	8.01	0.02	7.77	0.03	7.49	0.06	7.34	0.04	6.88	0.03
84.....	G307.8593+00.0448	O8F	9.31	9.66	7.87	0.02	7.69	0.04	7.58	0.02	7.43	0.04	7.51	0.05	7.45	0.04	7.31	0.03
85.....	G308.2587+00.3399	B3 V	10.84	11.05	10.40	0.02	10.37	0.02	10.34	0.02	10.22	0.05	10.27	0.05	10.31	0.06	9.79	0.06
86.....	G309.1551−00.7193	B	7.92	8.00	7.35	0.03	7.18	0.03	6.95	0.02	[a]	...	[a]	...	6.11	0.03	5.77	0.04
87.....	G309.9125−00.6853	O/BE	8.00	8.06	7.22	0.03	7.13	0.04	6.93	0.03	[a]	...	6.64	0.10	6.35	0.03	5.99	0.03
88.....	G311.3308−00.9293	O/BE	9.40	9.67	8.78	0.02	8.60	0.04	8.38	0.03	7.68	0.04	7.47	0.04	7.22	0.04	6.91	0.02
89.....	G311.3480−00.8498	O/BE	9.03	9.29	7.89	0.02	7.68	0.04	7.40	0.04	[a]	...	6.82	0.05	6.57	0.03	6.23	0.04
90.....	G313.2647+00.3411	O9/B0 (VN	9.08	9.26	8.49	0.02	8.44	0.03	8.41	0.02	8.18	0.04	8.35	0.06	8.32	0.03	8.17	0.03
91.....	G313.4496−00.0347	O9.5 V	7.99	8.17	7.34	0.03	7.31	0.04	7.27	0.02	7.27	0.04	7.32	0.05	7.24	0.04	7.13	0.03
92.....	G313.5404+00.1371	O9/9.5	8.40	8.79	7.10	0.02	6.99	0.05	6.86	0.02	[a]	...	6.78	0.06	6.63	0.03	6.45	0.04
93.....	G313.9455−00.4707	B3/5	9.47	9.67	9.00	0.03	8.97	0.02	8.90	0.02	8.33	0.04	8.28	0.04	8.05	0.03	7.73	0.03
94.....	G315.2130−00.6438	B1/2 VNE	7.61	7.69	7.06	0.02	6.93	0.03	6.66	0.02	[a]	...	[a]	...	5.89	0.04	5.61	0.03
95.....	G316.1548+00.1213	B3 VNE	9.13	9.26	8.50	0.02	8.45	0.04	8.34	0.03	8.20	0.04	8.12	0.06	7.97	0.04	7.65	0.03

TABLE 3—*Continued*

Table (1)	ID (2)	Spectral Type (3)	V (mag) (4)	B (mag) (5)	J (mag) (6)	$[J]\sigma$ (mag) (7)	H (mag) (8)	$[H]\sigma$ (mag) (9)	K (mag) (10)	$[K]\sigma$ (mag) (11)	[3.6] (mag) (12)	σ[3.6] (mag) (13)	[4.5] (mag) (14)	σ[4.5] (mag) (15)	[5.8] (mag) (16)	σ[5.8] (mag) (17)	[8.0] (mag) (18)	σ[8.0] (mag) (19)
96.....	G316.4591−00.3255	B3 IAB	10.88	11.12	9.61	0.03	9.42	0.02	9.19	0.03	8.87	0.05	8.77	0.06	8.61	0.04	8.16	0.04
97.....	G316.6434−00.7151	B9/A0 II/	10.73	10.91	10.12	0.02	10.01	0.02	10.01	0.02	10.01	0.04	10.01	0.04	9.97	0.05	9.75	0.06
98.....	G316.7608+00.0224	O6	10.75	11.44	9.23	0.03	9.04	0.02	8.94	0.02	8.86	0.05	8.81	0.06	8.75	0.04	8.43	0.04
99.....	G317.2161−00.7686	BE	10.10	10.65	7.94	0.03	7.62	0.05	7.28	0.03	[a]	...	6.58	0.05	6.28	0.04	5.86	0.03
100.....	G320.7229+00.2569	O9.5 IA	10.63	11.45	7.65	0.03	7.35	0.02	7.12	0.02	[a]	...	6.94	0.05	6.74	0.04	6.64	0.03
101.....	G321.1836+00.5562	B1 IA	10.56	11.88	6.50	0.02	6.07	0.03	5.77	0.02	[a]	...	[a]	...	5.46	0.04	5.33	0.02
102.....	G321.5613+00.5656	B8 III/IV	9.75	9.93	9.23	0.02	9.13	0.02	9.09	0.02	9.05	0.04	9.06	0.05	8.93	0.04	8.68	0.04
103.....	G323.8402−00.9095	B7 III	8.61	8.80	7.75	0.03	7.70	0.05	7.60	0.03	[a]	...	7.44	0.04	7.27	0.03	7.03	0.02
104.....	G324.6947−00.0606	A0 III/IV	9.92	10.05	9.38	0.03	9.33	0.03	9.24	0.02	9.20	0.03	9.26	0.04	9.16	0.03	8.97	0.04
105.....	G325.5031−00.3089	A0 III/IV	10.28	10.51	9.37	0.03	9.21	0.02	9.18	0.02	9.09	0.04	9.17	0.05	9.06	0.05	8.91	0.06
106.....	G326.2445+00.2388	B3 IV	10.47	10.77	8.99	0.03	8.89	0.05	8.74	0.02	...	...	...	...	8.29	0.05	8.13	0.04
107.....	G326.3079+00.7435	O4 III	11.40	12.61	7.47	0.03	7.07	0.03	6.86	0.02	[a]	...	6.68	0.04	6.59	0.04	6.43	0.02
108.....	G326.9420−00.0095	B2/3 VNNE	7.91	7.87	7.81	0.02	7.76	0.06	7.60	0.02	7.19	0.05	7.16	0.05	6.93	0.05	6.66	0.04
109.....	G327.8989−00.2804	B1 IB	9.34	9.75	7.91	0.02	7.80	0.04	7.73	0.02	7.62	0.04	7.73	0.03	7.64	0.04	7.57	0.03
110.....	G327.9524−00.7556	B1 IA/IAB	8.06	8.52	6.59	0.02	6.41	0.03	6.32	0.02	[a]	...	[a]	...	6.22	0.04	6.05	0.03
111.....	G329.3866+00.0615	B8 III	9.70	9.90	8.94	0.03	8.85	0.03	8.74	0.02	8.52	0.05	8.52	0.07	8.43	0.04	8.14	0.03
112.....	G330.8138−00.1170	B2 (IB)NE	9.53	9.81	8.56	0.02	8.46	0.04	8.46	0.03	8.13	0.04	8.19	0.06	8.12	0.04	7.89	0.03
113.....	G331.0318−00.1870	B5/7 (V)N	9.94	9.97	9.50	0.02	9.43	0.03	9.40	0.02	9.31	0.04	9.44	0.06	9.36	0.08	8.93	0.14
114.....	G331.3526−00.9401	B0.5 IA	10.54	11.38	8.41	0.03	8.19	0.04	8.02	0.03	7.84	0.04	7.83	0.06	7.75	0.05	7.68	0.03
115.....	G331.6345−00.9777	B0.5 IB	10.05	10.79	8.13	0.02	7.92	0.02	7.81	0.02	7.64	0.04	7.68	0.06	7.60	0.04	7.54	0.03
116.....	G331.6984−00.9605	B1 I	10.08	10.90	7.87	0.03	7.64	0.03	7.49	0.03	7.33	0.04	7.36	0.04	7.26	0.03	7.21	0.03
117.....	G332.2253−00.0986	B	9.79	9.99	8.85	0.02	8.80	0.03	8.79	0.02	8.77	0.03	8.78	0.04	8.68	0.06	8.55	0.08
118.....	G332.5918+00.0038	B (I)	10.48	10.71	9.64	0.02	9.50	0.02	9.48	0.02	9.36	0.04	9.49	0.05	9.41	0.06	9.32	0.05
119.....	G332.7690+00.8861	B7 III	8.67	8.80	8.03	0.03	8.05	0.03	7.95	0.03	7.85	0.03	7.92	0.04	7.85	0.03	7.70	0.03
120.....	G333.6850+00.6730	B2 VNE	7.61	7.66	7.15	0.02	7.09	0.04	6.93	0.03	[a]	...	[a]	...	6.04	0.04	5.74	0.03
121.....	G333.7353+00.6342	B5/7 (VN)	7.30	7.32	7.05	0.02	7.03	0.04	6.92	0.03	[a]	...	6.72	0.04	6.55	0.04	6.23	0.03
122.....	G334.4262−00.1817	B0 IA	10.02	10.68	8.01	0.02	7.78	0.04	7.66	0.02	7.54	0.09	7.59	0.06	7.46	0.05	7.43	0.03
123.....	G336.3661−00.2181	O6F	6.83	7.06	5.87	0.02	5.74	0.03	5.64	0.02	[a]	...	[a]	...	5.34	0.04	5.25	0.03
124.....	G336.7700−00.8225	B2/3 VNNE	9.02	9.11	8.92	0.03	8.85	0.02	8.72	0.02	8.38	0.04	8.28	0.05	8.11	0.05	7.63	0.02
125.....	G337.2680+00.4366	B9/A0 IAB	7.49	7.86	6.10	0.03	5.92	0.03	5.77	0.02	[a]	...	[a]	...	5.60	0.02	5.59	0.03
126.....	G338.1284−00.5392	B2 (I)N	8.73	8.85	8.13	0.02	8.01	0.02	7.81	0.02	7.36	0.02	7.27	0.04	7.06	0.02	6.83	0.02
127.....	G338.3332−00.4985	B3 IV	10.60	10.92	9.48	0.02	9.38	0.02	9.28	0.02	8.96	0.03	8.94	0.04	8.90	0.05	8.66	0.03
128.....	G338.6076−00.3140	B1/2NE	9.03	9.19	8.05	0.02	7.92	0.04	7.62	0.02	7.08	0.05	[a]	...	6.58	0.05	6.31	0.04
129.....	G338.9943−00.5927	A0 II	8.46	8.86	7.01	0.02	6.82	0.02	6.75	0.02	7.03	0.11	6.62	0.05	6.68	0.03	6.57	0.03
130.....	G339.5071−00.4100	O9.5 IAB	8.86	9.37	7.28	0.02	7.17	0.04	7.02	0.02	[a]	...	6.79	0.04	6.86	0.04	6.74	0.02
131.....	G341.1134−00.9408	O5/6FE	8.26	8.68	6.76	0.02	6.62	0.03	6.47	0.02	[a]	...	[a]	...	6.03	0.03	5.77	0.02
132.....	G343.0383−00.5193	B3 II/III	8.15	8.31	7.61	0.02	7.54	0.05	7.47	0.02	7.44	0.04	7.40	0.06	7.30	0.04	7.16	0.03
133.....	G343.3618+00.8883	B0 IB/II	6.38	6.69	...	...	5.22	0.05	5.06	0.02	[a]	...	[a]	...	4.93	0.04	4.80	0.02
134.....	G343.8034−00.0300	O/BE	9.15	9.58	7.45	0.03	7.09	0.04	6.73	0.02	[a]	...	[a]	...	5.67	0.04	5.29	0.02
135.....	G347.8578+00.7375	B(2)NE	9.19	9.51	7.82	0.02	7.59	0.03	7.27	0.03	[a]	...	6.64	0.06	6.44	0.03	6.04	0.03
136.....	G348.7274−00.7957	O F	11.91	12.75	7.64	0.02	7.21	0.02	6.90	0.02	[a]	...	[a]	...	6.39	0.04	6.21	0.03
137.....	G349.0551−00.9834	B2NE	8.77	8.90	8.03	0.02	7.85	0.02	7.66	0.03	7.15	0.05	6.98	0.05	6.77	0.04	6.34	0.04
138.....	G349.4258−00.3805	B2 (V)NE	7.90	8.03	7.11	0.02	7.01	0.02	6.79	0.02	[a]	...	[a]	...	6.05	0.04	5.66	0.04
139.....	G349.6027−00.8926	B0.5 IIIN	11.20	11.81	9.14	0.02	8.80	0.02	8.48	0.02	8.36	0.04	8.11	0.05	7.88	0.05	7.39	0.03

NOTES.—Col. (1): Table number. Col. (2): GLIMPSE ID number. Col. (3): Spectral type from Tycho-2 Spectral Catalog. Col. (4): V magnitude. Col. (5): B magnitude. Col. (6): 2MASS J magnitude. Col. (7): 1 σ uncertainty for J. Col. (8): 2MASS H magnitude. Col. (9): 1 σ uncertainty for H. Col. (10): 2MASS K magnitude. Col. (11): 1 σ uncertainty for K. Col. (12): [3.6] magnitude. Col. (13): 1 σ uncertainty for [3.6]. Col. (14): [4.5] magnitude. Col. (15): 1 σ uncertainty for [4.5]. Col. (16): [5.8] magnitude. Col. (17): 1 σ uncertainty for [5.8]. Col. (18): [8.0] magnitude. Col. (19): 1 σ uncertainty for [8.0].

[a] Saturated band not nondetection.

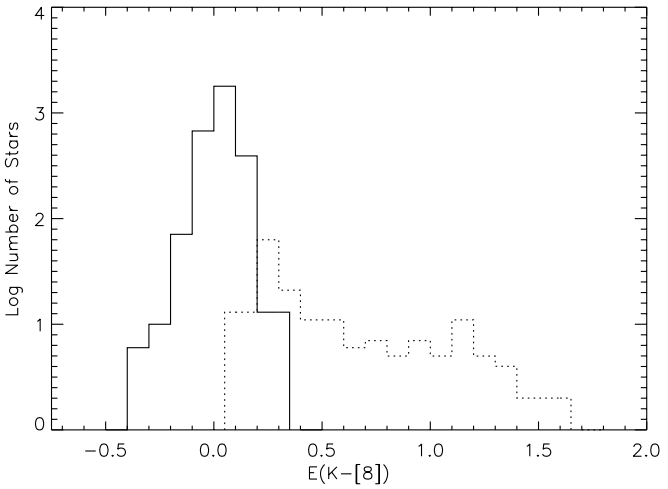

FIG. 2.—Histograms of $E(K - [8.0])$ for both mid-IR excess (*dotted*) and nonexcess (*solid*) stars from the GLIMPSE sample. The excess sources form a positive tail to the distribution of nonexcess sources. The overlap between the two distributions is a result of photometric uncertainties.

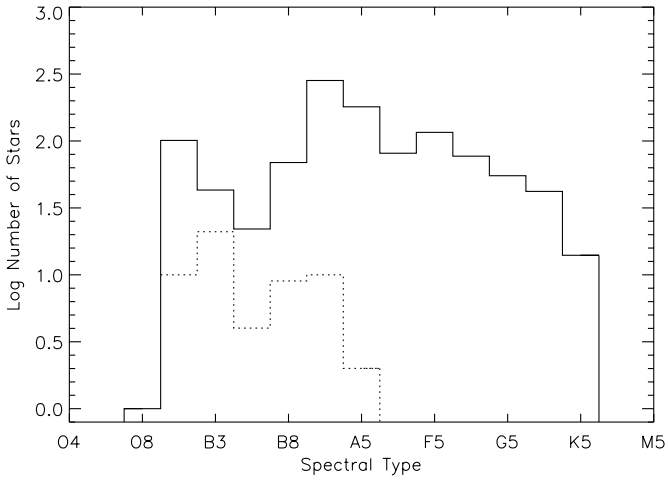

FIG. 4.—Histograms of main-sequence excess (*dotted*) and nonexcess (*solid*) sources by spectral type from the GLIMPSE sample. The distribution is broad and peaks near A0 for the nonexcess sources. The majority of the excess sources are earlier than A5.

ruled out. However, there is an argument against some unrelated background source that appears only at 8 μm or longer wavelengths (e.g., highly reddened stars or dusty post-AGB stars or protostars). If such sources were the case for the majority of objects, we would expect the histogram of excess objects in Figure 4 to look just like the histogram of all Tycho-2 Spectral Catalog sources; that is, the excesses should be randomly distributed across all spectral types. The fact that the excess stars are preferentially A and late B stars, the very objects where hot dust is most likely to be seen, argues against a large fraction of excesses due to source confusion in the beam.

Another possible origin for an excess is a pre–main-sequence circumstellar disk. During pre–main-sequence stellar evolution, stars accrete circumstellar material via equatorial disks that produce near-IR excesses. Figure 8 shows a $B - V$ versus $H - K$ color-color plot of the 47 sources from Tables 2 and 4 (i.e., B8 and later). GLIMPSE stars are the filled circles and *MSX* stars are triangles. The main sequence is shown by the dotted line, while the reddening vector for $A_V = 1$ is shown by the arrow.

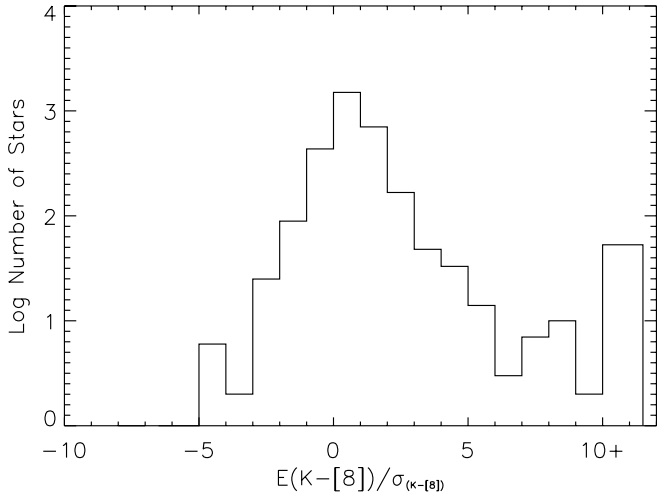

FIG. 3.—Histograms of the uncertainty distribution for 3086 GLIMPSE objects. The distribution is approximately Gaussian with a substantial positive tail. Only 10 stars have $E(K - [8.0])/\sigma_{(K-[8.0])} \leq -3$, consistent with the expectations of a normal error distribution. The 167 stars with $E(K - [8.0])/\sigma_{(K-[8.0])} \geq 3$ are listed in Tables 2 and 3.

With the exception of six objects, discussed in § 5.2, most stars are consistent with having no near-IR excess. Since the remaining 41 stars do not have a near-IR excess, the mid-IR excess is likely to arise within either a dissipating pre–main-sequence disk or a debris disk.

4. CONFIRMING THE EXCESSES AT 24 μm AND IDENTIFYING FALSE EXCESSES

We performed PSF-fitting photometry on post–basic calibrated data from the MIPSGAL survey (S14.4) on images containing mid-IR excess sources. We utilized IRAF/DAOPHOT point-source fitting with an aperture size of 15 pixels (36.8″) and an aperture correction factor of 1.08 that we obtained by interpolating Table 3.13 of the MIPS Data Handbook version 3.2.1. We matched the [24] sources to GLIMPSE/*MSX* sources using an 8″ search radius. We modeled the sources with the additional [24] measurement to determine $E(K - [24])$. This was determined in the same manner as $E(K - [8.0])$. We adopt 10% as an absolute calibration uncertainty on the [24] data (MIPS Data Handbook).

We detected 22 of the 28 GLIMPSE sources and were able to put upper limits on three of the GLIMPSE sources. The upper limits were calculated using $3 \times (\text{rms pixel}^{-1}) \times N_{\text{pix}}^{1/2}$, where N_{pix} is the aperture area of 707 pixels. Three sources were in regions not yet available in the *Spitzer* archives. Twenty sources detected at [24] had a measurement above the expected photosphere, but not all exhibited an excess at the 3 σ or greater level. Two sources, G042.9876+00.4201 and G322.6930+00.0572, were found to have photospheric [24] measurements. Given that we expect 6% of our 167-star excess sample (0.3% of the total GLIMPSE sample) to exhibit a false excess due to statistical deviations, 1–2 of the 28 excess GLIMPSE stars later than B8 should exhibit a false excess. Also, given that we would expect at most 4% (7 of 167 stars) to have excesses due to source correlation mismatches, we expect that 1 of the 28 excess GLIMPSE stars may be spurious. Therefore, we expect that 2–3 of the 28 GLIMPSE excess sources may be false excesses. Given that we have identified the two aforementioned sources as false [8.0] excesses, we feel that we have identified all the false [8.0] excesses among the 28 GLIMPSE sources in Tables 2 and 6. Two *MSX* sources with mid-IR excesses were within the MIPSGAL survey region and shown to be false excess sources as well. The false sources are discussed individually in § 5.3. We modeled the disk temperatures

TABLE 4

PHOTOMETRIC PARAMETERS FOR MAIN-SEQUENCE STARS B8 OR LATER WITH MID-IR EXCESSES FROM *MSX*

Table (1)	ID (2)	Spectral Type (3)	V (mag) (4)	B (mag) (5)	J (mag) (6)	$[J]\sigma$ (mag) (7)	H (mag) (8)	$[H]\sigma$ (mag) (9)	K (mag) (10)	$[K]\sigma$ (mag) (11)	*MSX* A (mag) (12)	σ A (%) (13)	*MSX* C (mag) (14)	σ C (%) (15)	*MSX* D (mag) (16)	σ D (%) (17)	*MSX* E (mag) (18)	σ E (%) (19)
1.....	G007.2369+01.4894	A1 V	6.88	6.97	6.20	0.02	5.53	0.04	4.78	0.02	1.55	4.10	0.66	5.00	0.50	6.10	−0.59	6.00
2.....	G008.3752−03.6697	F3 V	9.15	9.79	7.32	0.02	6.93	0.03	6.40	0.02	3.31	4.10	2.40	5.60	2.26	6.50	1.93	8.50
3.....	G009.4973+05.2441	A7 V	7.60	7.86	6.76	0.02	6.60	0.03	6.54	0.02	5.96	6.30	...	...	...	...	...	...
4.....	G025.6122+01.3020	B9 V	6.36	6.39	6.21	0.02	6.18	0.04	6.16	0.02	5.74	4.90	...	...	...	...	...	...
5.....	G040.9995−00.0423	F5 V	7.22	7.56	6.47	0.02	6.36	0.02	6.30	0.02	5.82	4.90	...	...	...	...	...	...
6.....	G042.0859−71.0408	A9 V	8.44	8.72	7.43	0.02	7.30	0.02	7.25	0.03	6.51	7.70	...	...	...	...	...	...
7.....	G054.5163+02.4470	K1 IV	7.32	8.49	5.10	0.02	4.53	0.04	6.51	0.05	4.33	4.20	3.21	46.20	...	...	...	...
8.....	G056.7848+00.8671	G8 V	9.34	10.76	6.76	0.03	6.12	0.02	5.96	0.02	5.09	4.40	...	...	...	...	...	...
9.....	G082.2118−02.7185	B8 V:NN	6.68	6.60	6.69	0.02	6.73	0.02	6.70	0.02	5.86	4.90	...	...	...	...	...	...
10.....	G201.9029−01.9739	B8 VN	6.20	6.15	6.32	0.02	6.34	0.05	6.31	0.02	5.84	5.30	...	...	...	...	0.52	30.40
11.....	G229.4514+01.0145	B9 IV	6.82	6.84	6.44	0.02	6.10	0.06	5.44	0.02	2.59	4.10	1.84	5.20	1.93	6.30	1.46	7.10
12.....	G257.6236+00.2459	A0 IV	8.61	8.62	8.43	0.02	8.28	0.04	7.91	0.02	3.91	4.10	2.96	6.10	2.56	6.50	1.31	6.60
13.....	G265.5536−03.9951	A5/7 V	7.79	8.06	7.11	0.03	6.96	0.03	6.92	0.02	6.36	7.70	...	...	...	...	...	...
14.....	G269.5873−05.8882	G0 V	8.84	9.52	7.24	0.02	6.87	0.02	6.76	0.02	6.11	4.90	...	...	...	...	...	...
15.....	G285.8890+01.2948	G8 IV	8.15	8.92	6.53	0.02	6.12	0.03	6.01	0.02	5.42	4.70	...	...	...	...	...	...
16.....	G294.1242+01.4656	B9/A0 V	9.32	9.49	8.64	0.02	8.22	0.05	7.47	0.03	3.46	4.10	2.53	5.70	2.13	6.40	1.29	6.90
17.....	G295.3770−02.6380	G2 V	8.18	8.75	6.98	0.02	6.71	0.03	6.62	0.02	6.15	6.20	...	...	...	...	...	...
18.....	G347.3777+04.2010	F5 V	9.29	9.97	7.68	0.03	7.06	0.03	6.50	0.02	3.67	4.20	3.01	7.90	2.71	7.70	1.02	7.10
19.....	G348.5129−00.1121	G0 V	6.06	6.59	4.91	0.02	4.64	0.02	4.55	0.02	3.85	4.10	2.54	5.50	1.64	6.10	1.15	6.40

NOTES.—Col. (1): Table number. Col. (2): *MSX* ID number. Col. (3): Spectral type from Tycho-2 Spectral Catalog. Col. (4): V magnitude. Col. (5): B magnitude. Col. (6): 2MASS J magnitude. Col. (7): 1 σ uncertainty for J. Col. (8): 2MASS H magnitude. Col. (9): 1 σ uncertainty for H. Col. (10): 2MASS K magnitude. Col. (11): 1 σ uncertainty for K. Col. (12): *MSX* A-band magnitude using zero points from Cohen et al. (2000). Col. (13): 1 σ percent flux density uncertainty for *MSX* A. Col. (14): *MSX* C-band magnitude. Col. (15): 1 σ percent flux density uncertainty for *MSX* C. Col. (16): *MSX* D-band magnitude. Col. (17): 1 σ percent flux density uncertainty for *MSX* D. Col. (18): *MSX* E-band magnitude. Col. (19): 1 σ percent flux density uncertainty for *MSX* E.

TABLE 5

PHOTOMETRIC PARAMETERS FOR MAIN-SEQUENCE STARS EARLIER THAN B8 WITH MID-IR EXCESSES FROM *MSX*

Table (1)	ID (2)	Spectral Type (3)	V (mag) (4)	B (mag) (5)	J (mag) (6)	$[J]\sigma$ (mag) (7)	H (mag) (8)	$[H]\sigma$ (mag) (9)	K (mag) (10)	$[K]\sigma$ (mag) (11)	*MSX* A (mag) (12)	σ A (%) (13)	*MSX* C (mag) (14)	σ C (%) (15)	*MSX* D (mag) (16)	σ D (%) (17)	*MSX* E (mag) (18)	σ E (%) (19)
1.....	G058.7278−00.4506	B2 V:NNE	10.07	10.39	8.90	0.02	8.78	0.02	8.49	0.02	6.93	7.50	3.43	53.90	...	...	...	...
2.....	G059.7235−02.0661	B3) IV	4.85	4.71	5.39	0.24	5.05	0.02	4.95	0.02	4.66	4.30	...	...	...	...	...	...
3.....	G065.5291−04.0730	B7 V(E)	5.88	5.78	5.97	0.02	6.05	0.02	6.00	0.02	5.40	4.60	...	...	...	...	...	...
4.....	G071.0310−01.6810	B1 V:PNNE	7.18	7.24	6.62	0.02	6.53	0.02	6.36	0.02	5.45	4.70	...	...	...	...	...	...
5.....	G073.0727+03.7595	B3 V	5.11	4.98	5.41	0.03	5.48	0.02	5.49	0.03	4.60	4.30	...	...	...	...	...	...
6.....	G073.9148+02.0441	B3 V	4.89	4.76	5.07	0.04	5.16	0.02	5.04	0.02	4.01	4.20	3.70	9.50	3.67	10.10	...	...
7.....	G074.2184+01.1861	B0 IV)	8.43	8.73	7.18	0.03	7.05	0.02	6.76	0.02	5.73	4.90	...	...	...	...	...	...
8.....	G074.8713+00.9892	B5 IV	6.43	6.34	6.51	0.02	6.55	0.01	6.57	0.02	6.10	5.40	...	...	...	...	...	...
9.....	G088.0296+00.9707	09 V)	4.73	4.64	4.66	0.27	4.46	0.08	4.34	0.34	3.57	4.10	3.49	6.30	3.02	6.60	...	...
10.....	G089.2686−04.9218	B2 V:NN(E)	7.62	7.58	7.65	0.02	7.64	0.02	7.52	0.02	6.06	6.70	...	...	...	...	...	...
11.....	G096.3764+03.5507	B1 VE	7.63	8.09	6.21	0.03	5.96	0.03	5.63	0.01	4.56	4.20	...	...	3.28	45.00	...	...
12.....	G099.5298+04.3982	B2 VNNE	8.61	8.96	7.54	0.02	7.48	0.02	7.28	0.02	6.03	6.60	...	...	...	...	...	...
13.....	G101.0774+01.2676	B6 V:N	8.34	8.54	7.45	0.03	7.12	0.03	6.46	0.02	3.89	4.10	3.37	7.50	3.61	9.40	...	...
14.....	G103.1147+04.2269	B1 V	7.71	7.95	6.85	0.04	6.71	0.06	6.49	0.02	5.95	5.70	...	...	...	...	...	...
15.....	G104.5663+01.2800	O9.5V	9.79	10.25	8.13	0.02	7.98	0.03	7.93	0.02	6.83	8.30	3.13	40.50	...	...	...	...
16.....	G126.6762+00.1946	B1:PE V)	10.69	11.43	8.43	0.02	8.13	0.02	7.81	0.02	6.45	6.10	...	...	...	...	...	...
17.....	G131.0706−02.5786	B 2 VNE	7.04	7.06	6.46	0.02	6.33	0.05	6.14	0.03	5.44	5.10	...	...	...	...	...	...
18.....	G145.2365−00.3173	B2 VNE	7.77	8.16	6.41	0.02	6.29	0.03	6.04	0.02	5.18	4.40	...	...	...	...	...	...
19.....	G148.3253−01.3348	B1 IV	7.02	7.25	6.16	0.02	6.11	0.03	6.00	0.02	5.50	4.60	...	...	...	...	...	...
20.....	G162.4782+01.5076	B5 V	9.42	9.96	7.60	0.03	7.48	0.02	7.33	0.02	5.56	4.70	...	...	3.38	8.40	...	...
21.....	G166.9465+00.6744	B2 V:PE	7.39	7.37	7.44	0.02	7.46	0.02	7.48	0.02	6.29	5.70	...	...	...	...	...	...
22.....	G169.1413−01.7258	B1 VE	8.16	8.35	7.69	0.02	7.66	0.02	7.53	0.02	5.92	5.50	...	...	...	...	...	...
23.....	G173.6026+02.7946	O9.5 V)	10.73	11.55	8.38	0.03	8.12	0.02	7.95	0.02	3.94	4.20	1.91	5.50	1.00	6.20	...	...
24.....	G182.9879+00.1386	B3 V	8.11	8.17	7.59	0.02	7.58	0.06	7.26	0.02	6.01	5.40	...	...	...	...	...	...

TABLE 5—*Continued*

Table (1)	ID (2)	Spectral Type (3)	V (mag) (4)	B (mag) (5)	J (mag) (6)	$[J]\sigma$ (mag) (7)	H (mag) (8)	$[H]\sigma$ (mag) (9)	K (mag) (10)	$[K]\sigma$ (mag) (11)	*MSX* A (mag) (12)	σ A (%) (13)	*MSX* C (mag) (14)	σ C (%) (15)	*MSX* D (mag) (16)	σ D (%) (17)	*MSX* E (mag) (18)	σ E (%) (19)
25.....	G190.9986−00.7868	B1 V:E	9.37	9.84	7.90	0.02	7.64	0.02	7.33	0.02	6.20	5.80	...	...	...	...	...	...
26.....	G194.0070−00.5432	B0,5 V:NNE	9.26	9.59	8.39	0.02	8.33	0.03	8.19	0.02	6.28	6.00	...	...	...	...	...	...
27.....	G196.3370+00.8012	B2 V	8.06	8.25	7.33	0.03	7.25	0.03	7.06	0.02	5.96	5.20	...	...	...	...	...	...
28.....	G208.4408+02.3883	B2 VE	6.92	6.93	6.62	0.02	6.53	0.04	6.29	0.03	4.95	4.60	...	...	...	...	...	...
29.....	G230.9053+03.0158	B2/3 V(N)	5.64	5.58	5.51	0.02	5.49	0.06	5.20	0.02	3.89	4.20	3.21	41.10	...	...	...	...
30.....	G231.0873−00.2140	B2 VNE	5.20	5.16	5.42	0.02	5.46	0.04	5.42	0.03	4.43	4.20	3.73	8.50	3.55	8.50	...	...
31.....	G231.3558+00.5087	B2 V)NE	8.51	8.62	7.87	0.03	7.80	0.04	7.54	0.03	6.40	6.30	...	...	...	...	...	...
32.....	G234.8252+02.9293	B3 V)NNE	8.39	8.44	7.74	0.03	7.45	0.05	6.89	0.02	4.95	4.60	...	...	...	...	...	...
33.....	G254.5364−02.6343	B3 V	6.33	6.28	6.20	0.02	6.17	0.03	6.05	0.02	5.34	4.90	...	...	...	...	...	...
34.....	G259.7707+24.1382	B5 V	6.13	6.04	6.32	0.02	6.35	0.03	6.23	0.02	5.02	4.20	4.53	10.70	...	...	...	...
35.....	G277.3806−00.4361	B3/5 VE	7.97	8.01	7.61	0.02	7.53	0.05	7.33	0.04	6.18	5.20	...	...	...	...	...	...
36.....	G306.6155−03.6706	B1 VPE	9.18	9.32	8.72	0.02	8.52	0.03	8.29	0.02	6.65	7.60	...	...	...	...	...	...
37.....	G314.1251+03.9597	B5 VNE	5.03	4.95	5.03	0.02	4.99	0.02	4.77	0.02	3.73	4.10	2.92	6.70	2.86	7.50	...	...
38.....	G315.2129−00.6435	B1/2 VNE	7.60	7.68	7.06	0.02	6.93	0.03	6.66	0.02	5.58	4.50	...	...	...	...	...	...
39.....	G328.0995+01.9428	B5/7 IV	7.06	7.02	6.96	0.03	6.95	0.03	6.86	0.02	5.58	4.80	...	...	...	...	...	...
40.....	G331.4496−01.8383	B5 IV/V	8.01	8.07	7.08	0.02	6.70	0.05	6.44	0.03	5.85	5.50	3.78	11.30	...	...	...	...
41.....	G333.7354+00.6343	B5/7 (VN)	7.29	7.32	7.05	0.02	7.03	0.04	6.92	0.03	6.22	5.70	...	...	...	...	...	...
42.....	G334.8738+01.2213	B7 V	6.49	6.45	6.58	0.02	6.64	0.04	6.62	0.03	6.19	5.90	...	...	...	...	...	...
43.....	G345.5396−02.3946	B2/3 V)NNE	6.97	7.03	6.20	0.02	6.12	0.03	5.99	0.02	4.92	4.30	...	...	...	...	...	...
44.....	G353.6612−01.9231	B2 VNE	8.26	8.60	6.80	0.02	6.60	0.03	6.34	0.03	5.11	4.50	...	...	...	...	...	...

NOTES.—Col. (1): Table number. Col. (2): *MSX* ID number. Col. (3): Spectral type from Tycho-2 Spectral Catalog. Col. (4): V magnitude. Col. (5): B magnitude. Col. (6): 2MASS J magnitude. Col. (7): 1 σ uncertainty for J. Col. (8): 2MASS H magnitude. Col. (9): 1 σ uncertainty for H. Col. (10): 2MASS K magnitude. Col. (11): 1 σ uncertainty for K. Col. (12): *MSX* A-band magnitude. Col. (13): 1 σ percent flux density uncertainty for *MSX* A. Col. (14): *MSX* C-band magnitude. Col. (15): 1 σ percent flux density uncertainty for *MSX* C. Col. (16): *MSX* D-band magnitude. Col. (17): 1 σ percent flux density uncertainty for *MSX* D. Col. (18): *MSX* E-band magnitude. Col. (19): 1 σ percent flux density uncertainty for *MSX* E.

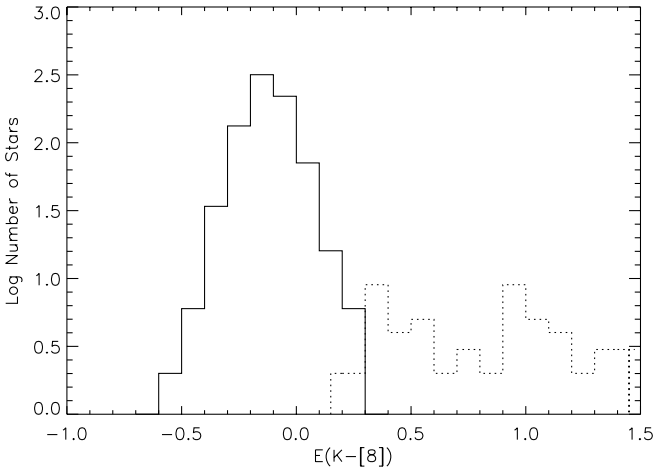

FIG. 5.—Histograms for main-sequence excess (*dotted*) and nonexcess (*solid*) sources from the *MSX* sample. The excess sources form a positive tail to the nonexcess distribution.

and fractional infrared luminosities for the 20 GLIMPSE sources having [24] excesses using all available photometry.

5. EXAMINING THE EXCESSES

5.1. *Modeling*

We modeled the SEDs of stars exhibiting mid-IR excesses (Tables 2 and 4) to estimate the stellar distances, extinctions, putative circumstellar disk temperatures, and fractional infrared luminosities. The photometric data points were fitted with Kurucz ATLAS9 models using temperatures and effective gravities corresponding to the nearest spectral type (Kurucz 1993). Since all of the stars lie within the solar circle, we adopt the solar metallicity models. The Kurucz model surface fluxes were scaled by a factor, X, so that the model K-band fluxes matched the observed K-band 2MASS photometry. This scale factor represents $X = R^2/D^2$, the ratio of the stellar radius squared over the distance to the star squared. Adopting stellar radii appropriate for the observed spectral types (Drilling & Landolt 2000), we calculated a spectrophotometric distance to each star. These distances and their uncertainties, estimated by taking into account

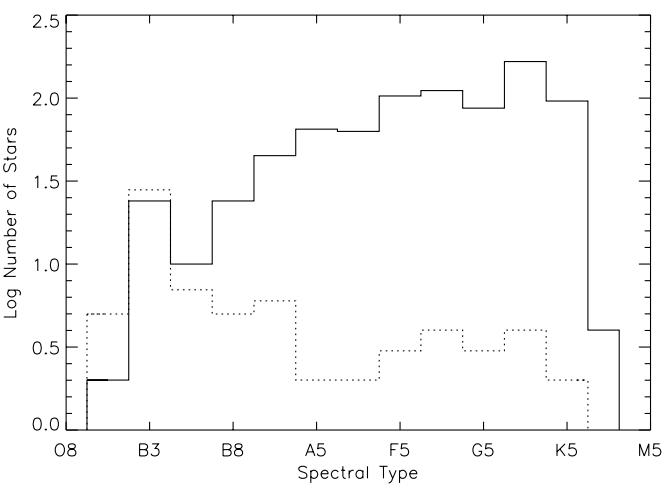

FIG. 6.—Histograms for main-sequence excess (*dotted*) and nonexcess (*solid*) sources by spectral type for the *MSX* sample. A larger fraction of the *MSX* sources are of later spectral type relative to the distribution of GLIMPSE sources in Fig. 4. For the earliest stars excesses are more common than not.

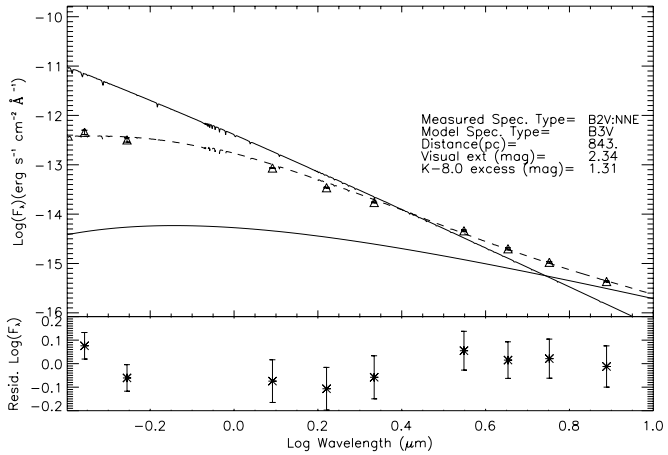

FIG. 7.—SED of an early B main-sequence star, G058.7277−00.4505, in which the IR excess is best explained by thermal bremsstrahlung emission. The Kurucz model for a B3 V star is shown by the thick solid line. The dot-dashed line is the thermal bremsstrahlung model component. The dashed line is the B3 V stellar model with applied extinction and the thermal bremsstrahlung component. The bottom panel shows the residuals from the Kurucz model after the inclusion of the bremsstrahlung component, extinction, and distance normalization.

the K-band photometric errors added in quadrature with an additional 15% uncertainty in the stellar radii, are listed in Table 7. The K-band measurements were used as the basis for the distance computation because the effects of extinction are nearly negligible at 2.2 μm for most of our stars. Our derived A_V values are all <2.5 mag, implying $A_K < 0.25$ mag, with most having $A_V < 1.0$. The model atmospheres were reddened with variable amounts of extinction using the Li & Draine (2001) extinction curve, except in the mid-infrared ($\lambda > 3$ μm), where the GLIMPSE extinction results were used (Indebetouw et al. 2005). Distance and extinction were fitted iteratively as free parameters covering a grid of all reasonable values. The best-fit parameters for each star are determined by the minimum of the χ^2 statistic. Modeling the star with the next earlier or later spectral type model available in the Kurucz library (i.e., an A3 with an A0 or an A5) produced similar reduced χ^2 values. This allows small errors in classification to yield similar results. This also provides a check on classification. If a star is grossly misclassified, the fit is poor,

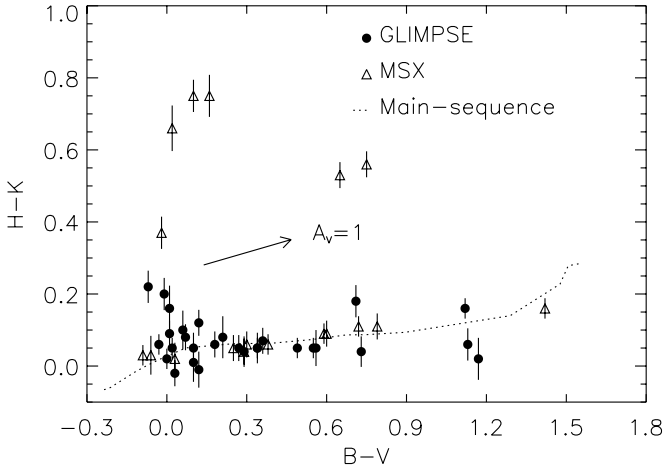

FIG. 8.—Color-color plot of $B - V$ vs. $H - K$ for excess sources B8 or later from GLIMPSE (*circles*) and *MSX* (*triangles*). The dotted line denotes the main sequence and the arrow shows the reddening vector for $A_V = 1$. Six stars show large near-IR excesses, $H - K > 0.3$; however, the majority (87%) of the stars from both samples are consistent with having minimal near-IR excess.

TABLE 6
24 μm Photometry

Table (1)	ID (2)	Spectral Type (3)	[24] (mJy) (4)	[24] (mag) (5)	σ [24] (mJy) (6)
1.....	G011.2691+00.4208	B9 V	18.4	6.47	0.3
2.....	G014.4239−00.7657	B8	71.9	4.99	13.5
3.....	G027.0268+00.7224	A0 V	17.7	6.51	1.1
4.....	G036.8722−00.4112	B8 V	21.7	6.29	0.5
5.....	G042.9876+00.4201	B8 V	4.7	7.95	0.2
6.....	G047.3677+00.6199	B8 Ve	44.6	5.51	0.8
7.....	G047.4523+00.5132	A0 V	8.5	7.31	0.7
8.....	G051.6491−00.1182	A0 V	17.8	6.51	2.3
9.....	G060.2596−00.5188	B8 V	71.3	5.00	16.2
10.....	G063.5770−00.3387	B9 V	29.3	5.97	4.0
11.....	G064.3921+00.0872	B8+G	5.0	7.89	0.1
12.....	G299.1677−00.3922	B8	7.0	7.52	0.5
13.....	G299.7090−00.9704	B8/9 IV	5.1	7.87	0.1
14.....	G300.0992−00.0627	A1	7.3	7.48	0.3
15.....	G305.1140−00.2353[a]	B8/9 V	<28.6		
16.....	G305.4232−00.8229	B6/8 V(E)	16.7	6.58	0.7
17.....	G307.9784−00.7148	B8 V(N)	21.5	6.30	0.7
18.....	G309.4316−00.3222[a]	B8 V	<40.4		
19.....	G310.5420+00.4120	B8 IV(N)	5.6	7.76	0.3
20.....	G311.0099+00.4156	A3 IV	149.4	4.20	4.2
21.....	G311.6185+00.2469	B8/9 IV/V	8.6	7.30	1.2
22.....	G314.3136−00.6977	A1 IV	22.8	6.24	0.4
23.....	G320.1546−00.7551[a]	B9.5 IV/V	<4.1		
24.....	G321.7868+00.4102	B8 VN	12.6	6.88	0.3
25.....	G322.6930+00.0572	F7/G0	3.7	8.21	0.3
26.....	G339.4392−00.7791[b]	A0/1 IV/V	...	...	...
27.....	G339.7415−00.1904[b]	A0	...	...	...
28.....	G340.0517+00.6687[b]	B8	...	...	...

Notes.— Col. (1): Table number. Col. (2): GLIMPSE ID number. Col. (3): Spectral type from Tycho-2 Spectral Catalog. Col. (4): [24] flux measurement in mJy. Col. (5): [24] measurement in magnitudes using 7.14 Jy zero point. Col. (6): 1 σ uncertainty for [24] in magnitudes.

[a] 3 σ upper limit.

[b] Data have not yet been released for this region of MIPSGAL.

resulting in photometric data becoming grossly inconsistent with the SED, and the classification is revisited.

To estimate the fractional infrared luminosities and temperatures of disks surrounding the mid-IR excess stars, we modeled the excess in each star as a single blackbody with the temperature and fractional infrared luminosity, $L_{\rm IR}/L_*$, as free parameters. This assumption, although simplistic, yields an approximation to the temperature and $L_{\rm IR}/L_*$ of the dust disks, given the limited number of photometric points available. We searched a grid of blackbody temperatures and fractional infrared luminosities to find best fits to the data. The temperature grid ranged from 50 to 1050 K in steps of 1 K. Because the IRAC data are sensitive only to the hottest dust in the inner portions of disks, fitting the mid-IR points in the absence of longer wavelength measurements essentially provides upper limits on the disk temperatures and fractional infrared luminosities. Chen & Jura (2001) found the color temperature of the disk around ζ Leporis to be 370 K using mid-IR data, but they note that fits including data at wavelengths longer than 10 μm indicate a disk temperature more consistent with a 230 K blackbody. Owing to this effect, we only model sources that were measured at [24], for GLIMPSE sources, or band C, D, or E in *MSX*, in addition to exhibiting an $E(K-[8.0])$.

We investigated the likelihood of other disk temperature/fractional infrared luminosity combinations using a Monte Carlo simulation to determine the uncertainties on our derived disk and star parameters. The Monte Carlo code adds noise to each of the photometric data points based on idealizations drawn from Gaussian models of their 1 σ photometric errors and then recomputes the most probable distance, visual extinction, blackbody temperature, and fractional infrared luminosity. We then used the linear distributions of key parameters from the simulations to determine their uncertainties.

Table 7 lists derived parameters and their uncertainties based on the median values of the Monte Carlo simulations for both the GLIMPSE and *MSX* excess sources B8 or later. Unfortunately, most *MSX* sources are detected only at A band, fall outside the MIPSGAL survey region, and were not modeled. Also in Table 7 is the measured radial separation between the optical and IR source.

Figures 9–13 show the SEDs of mid-IR excess sources in GLIMPSE that are confirmed in MIPSGAL. The Kurucz model atmosphere is shown by the thick solid line, the model atmosphere with applied extinction is the dashed line, the dot-dashed line is the blackbody representing the disk, and the thin solid line is the sum of the extincted model atmosphere and the applied blackbody. The plot below each SED shows residuals from the best-fit model. In most cases, the single-temperature blackbody component provides a good fit to the data. The approximately four sources that are not well modeled by a single-temperature blackbody will be discussed in § 5.3. In most cases, a plausible explanation for the poor fits is the existence of multiple temperature (i.e., cooler) components within the disks that contribute to the excesses at wavelengths $\lambda \geq 8$ μm.

Figure 14 shows a summary histogram of all model disk temperatures and fractional infrared luminosities. Disk temperatures are broadly peaked at ~450 K but span a range from ~190 to 800 K. Assuming blackbody radiation, an estimation of the inner radius for circumstellar material can be made and is found to range from 0.4 to 27 AU for these sources. The majority of the sources have inner radii of 1–6 AU for the late B and early A stars of our sample. The distribution of fractional infrared luminosities is bimodal, having peaks near 10^{-3} and 10^{-1}. The majority of stars have fractional infrared luminosities between 10^{-3} and 10^{-2}. Figure 14 clearly shows that we have two different populations of mid-IR sources, with one or two sources that bridge this gap.

5.2. *Protostellar Disks or Debris Disks?*

Lagrange et al. (2000) suggested a definition of debris disks using four criteria. These criteria require that the fractional infrared luminosity is small, i.e., $L_{\rm IR}/L_* \leq 10^{-3}$, the mass of the gas and dust must be below 10^{-2} $M_\odot$, the dust mass must be significantly greater than the gas mass, and the grain destruction time must be much less than the stellar age. Our limited data only allow comparisons based on the fractional infrared luminosities. Artymowicz (1996) gives a more liberal criterion, allowing maximum fractional infrared luminosities of $L_{\rm IR}/L_* < 10^{-2}$ for debris disks. Protostars, on the other hand, have $L_{\rm IR}/L_* \geq 0.1$ (e.g., Baud et al. 1984).

Six stars exhibit fractional infrared luminosities less than or equal to 10^{-3} and have fractional infrared luminosities consistent with being debris disks. Six stars have $L_{\rm IR}/L_* > 5 \times 10^{-2}$ and are almost certainly Class II protostars. The majority of our sample (14 stars) have $10^{-3} < L_{\rm IR}/L_* < 10^{-2}$ and are consistent with either transition disks in late-stage protostars or massive debris disks.

Optical spectra can be used to further discriminate between the pre–main-sequence and debris disk nature of the IR excess. Pre–main-sequence stars exhibit Balmer emission produced by

TABLE 7

DERIVED PARAMETERS FOR MID-IR EXCESS SOURCES LATER THAN B8 IN GLIMPSE AND *MSX*

Table (1)	ID (2)	Spectral Type (3)	HD (4)	$E(K-[8.0])$ (mag) (5)	$E(K-[8.0])/\sigma_{(K-[8.0])}$ (6)	Distance (pc) (7)	A_V (mag) (8)	T (K) (9)	L_{IR}/L_* (10)	T_{eff} (K) (11)	$\log g$ (12)	R (arcsec) (13)	Comments (14)
1.....	G007.2369+01.4894	A1 V	163296	2.96	64.89	63^{+10}_{-10}	$2.09^{+0.01}_{-1.05}$	493^{+4}_{-5}	$0.14^{+0.002}_{-0.002}$	8200	+4.29	0.8	M, e, p, o, x, c, g
2.....	G008.3752−03.6697	F3 V	167905	2.82	61.82	53^{+10}_{-10}	$1.76^{+0.01}_{-0.01}$	566^{+7}_{-8}	$0.20^{+0.004}_{-0.005}$	6440	+4.34	0.6	M, o, c, g
3.....	G011.2691+00.4208	B9 V	165854	0.34	4.52	278^{+45}_{-45}	$0.52^{+0.06}_{-0.06}$	473^{+13}_{-14}	$0.0010^{+0.0001}_{-0.0001}$	9520	+4.14	0.6	G, e
4.....	G014.4239−00.7657	B8	168246	0.48	4.25	1008^{+155}_{-155}	$0.93^{+0.05}_{-0.06}$	191^{+5}_{-4}	$0.013^{+0.001}_{-0.001}$	11900	+4.04	0.6	G
5.....	G027.0268+00.7224	A0 V	172030	0.22	3.68	208^{+35}_{-35}	$2.22^{+0.13}_{-0.13}$	486^{+17}_{-19}	$0.0014^{+0.0001}_{-0.0002}$	9520	+4.14	0.4	G, e
6.....	G036.8722−00.4112	B8 V	...	0.26	4.09	323^{+50}_{-50}	$1.24^{+0.07}_{-0.07}$	388^{+11}_{-10}	$0.0013^{+0.0001}_{-0.0001}$	11900	+4.04	0.3	G
7.....	G047.3677+00.6199[a]	B8 Ve	180398	0.95	15.98	318^{+50}_{-50}	$0.55^{+0.07}_{-0.03}$	787^{+20}_{-16}	$0.0034^{+0.0001}_{-0.0002}$	11900	+4.14	0.4	G, e
8.....	G047.4523+00.5132	A0 V	231033	0.26	4.08	438^{+70}_{-70}	$0.98^{+0.06}_{-0.05}$	355^{+8}_{-8}	$0.0012^{+0.0001}_{-0.0001}$	9520	+4.14	0.5	G
9.....	G051.6491−00.1182	A0 V	183035	0.20	3.21	283^{+45}_{-45}	$0.32^{+0.04}_{-0.05}$	360^{+13}_{-13}	$0.00052^{+0.00004}_{-0.00005}$	9520	+4.14	0.5	G
10.....	G060.2596−00.5188	B8 V	344882	0.79	8.48	598^{+90}_{-90}	$0.49^{+0.06}_{-0.06}$	252^{+9}_{-5}	$0.0041^{+0.0003}_{-0.0004}$	11900	+4.04	0.5	G
11.....	G063.5770−00.3387[a]	B9 V	339086	0.32	5.07	463^{+70}_{-70}	$0.87^{+0.06}_{-0.05}$	302^{+2}_{-3}	$0.0020^{+0.0001}_{-0.0001}$	9520	+4.14	0.5	G
12.....	G064.3921+00.0872	B8+G	333048	0.29	4.89	498^{+75}_{-75}	$1.76^{+0.10}_{-0.01}$	599^{+16}_{-14}	$0.0016^{+0.0001}_{-0.0002}$	11900	+4.04	0.5	G
13.....	G229.4514+01.0145	B9 V	58647	2.63	57.65	88^{+15}_{-15}	$1.39^{+0.01}_{-0.08}$	579^{+4}_{-5}	$0.058^{+0.001}_{-0.001}$	9520	+4.14	1.3	M, e, o, c, g
14.....	G257.6236+00.2459	A0 IV	72106	3.83	83.96	288^{+45}_{-55}	$0.69^{+0.04}_{-0.03}$	404^{+9}_{-10}	$0.12^{+0.002}_{-0.002}$	9520	+4.14	1.5	M, m, p, o, g
15.....	G294.1242+01.4656	B9/A0 V	101412	3.75	73.81	218^{+35}_{-35}	$1.86^{+0.01}_{-0.01}$	433^{+8}_{-8}	$0.27^{+0.004}_{-0.006}$	9520	+4.14	0.2	M, e, p, o, c, g
16.....	G299.1677−00.3922	B8	...	0.38	5.34	593^{+90}_{-90}	$0.62^{+0.07}_{-0.07}$	442^{+26}_{-14}	$0.00082^{+0.00008}_{-0.00005}$	11900	+4.04	0.4	G
17.....	G299.7090−00.9704	B8/9 IV	107609	0.20	3.08	448^{+70}_{-70}	$0.58^{+0.07}_{-0.06}$	432^{+45}_{-31}	$0.00051^{+0.00006}_{-0.00007}$	9520	+4.14	0.5	G, e
18.....	G300.0992−00.0627	A1	...	0.53	8.18	333^{+55}_{-55}	$0.39^{+0.04}_{-0.05}$	501^{+79}_{-28}	$0.0026^{+0.0001}_{-0.0001}$	8200	+4.29	0.4	G, e
19.....	G305.4232−00.8229[a]	B6/8 V(E)	114757	0.79	12.89	483^{+75}_{-75}	$0.98^{+0.06}_{-0.05}$	668^{+41}_{-34}	$0.0037^{+0.0003}_{-0.0002}$	11900	+4.04	0.4	G, e
20.....	G307.9784−00.7148	B8 V (N)	118094	0.45	6.29	333^{+50}_{-50}	$0.46^{+0.06}_{-0.05}$	555^{+22}_{-19}	$0.00087^{+0.00007}_{-0.00005}$	11900	+4.04	0.2	G, e
21.....	G310.5420+00.4120	B8 IV(N)	121195	0.28	4.18	508^{+80}_{-80}	$0.62^{+0.07}_{-0.04}$	442^{+18}_{-12}	$0.00039^{+0.00003}_{-0.00005}$	11900	+4.04	0.3	G, e
22.....	G311.0099+00.4156[a]	A3 IV	121808	0.37	4.24	128^{+20}_{-20}	$0.52^{+0.06}_{-0.03}$	315^{+4}_{-3}	$0.0027^{+0.0001}_{-0.0003}$	8200	+4.29	0.5	G
23.....	G311.6185+00.2469	B8/9 IV/V	122620	0.27	3.79	578^{+90}_{-90}	$0.55^{+0.07}_{-0.06}$	308^{+11}_{-7}	$0.0012^{+0.0001}_{-0.0001}$	9520	+4.14	0.2	G
24.....	G314.3136−00.6977	A1 IV	126578	0.21	3.39	168^{+30}_{-30}	$0.32^{+0.04}_{-0.05}$	328^{+7}_{-13}	$0.00096^{+0.00006}_{-0.00006}$	8200	+4.29	0.4	G
25.....	G321.7868+00.4102	B8 V N	135354	0.80	11.96	553^{+85}_{-85}	$0.58^{+0.07}_{-0.06}$	583^{+18}_{-21}	$0.0021^{+0.0002}_{-0.0001}$	11900	+4.04	0.3	G, e
26.....	G347.3777+04.2010	F5 V	152404	2.56	55.03	53^{+10}_{-10}	$1.86^{+0.11}_{-1.86}$	487^{+9}_{-11}	$0.13^{+0.02}_{-0.03}$	6440	+4.34	0.3	M, e, o, c, g
27.....	G305.1140−00.2353	B8/9 V	114277	0.19	3.06	458^{+70}_{-70}	$1.10^{+0.07}_{-0.06}$	...	...	9520	+4.14	0.4	G

TABLE 7—*Continued*

Table (1)	ID (2)	Spectral Type (3)	HD (4)	$E(K-[8.0])$ (mag) (5)	$E(K-[8.0])/\sigma_{(K-[8.0])}$ (6)	Distance (pc) (7)	A_V (mag) (8)	T (K) (9)	L_{IR}/L_* (10)	T_{eff} (K) (11)	log g (12)	R (arcsec) (13)	Comments (14)
28.....	G309.4316−00.3222	B8 V	119940	0.29	3.74	763^{+115}_{-115}	$0.58^{+0.07}_{-0.06}$	...	...	11900	+4.04	0.3	G, e
29.....	G320.1546−00.7551	B9.5 IV/V	134203	0.26	3.18	568^{+90}_{-90}	$0.62^{+0.07}_{-0.07}$	...	...	9520	+4.14	0.4	G
30.....	G009.4973+05.2441[b]	A7 V	161643	0.39	5.90	73^{+15}_{-15}	$0.39^{+0.02}_{-0.02}$	...	...	7200	+4.34	1.1	M, m, c
31.....	G025.6122+01.3020[b]	B9 V	171149	0.28	5.29	133^{+20}_{-20}	$0.22^{+0.01}_{-0.01}$	...	...	9520	+4.14	0.6	M
32.....	G040.9995−00.0423[c]	F5 V	177904	0.33	6.24	58^{+10}_{-10}	$0.00^{+0.01}_{-0.00}$	...	...	6440	+4.34	1.4	M, m, c
33.....	G042.0859−71.0408[b]	A9 V	221199	0.57	6.90	103^{+20}_{-20}	$0.49^{+0.03}_{-0.03}$	...	...	7200	+4.34	1.1	M, m, c
34.....	G042.9876+00.4201[c]	B8 V	178479	0.51	7.76	378^{+60}_{-60}	$1.31^{+0.08}_{-0.07}$	...	...	11900	+4.04	0.4	G, e
35.....	G054.5163+02.4470[b]	K1 V	182293	1.94	29.71	38^{+10}_{-10}	$0.00^{+0.01}_{-0.00}$	...	...	5250	+4.49	1.2	M
36.....	G056.7848+00.8671[c]	G8 V	334593	0.55	11.38	23^{+5}_{-5}	$2.09^{+0.01}_{-1.99}$	...	...	5250	+4.49	1.0	M, c
37.....	G082.2118−02.7185[b]	B8 V:NN	199218	0.73	13.79	208^{+35}_{-35}	$0.20^{+0.01}_{-0.01}$	...	...	11900	+4.04	1.2	M, e, x, c
38.....	G201.9029−01.9739[d]	B8 VN	44783	0.37	6.53	173^{+30}_{-30}	$0.15^{+0.01}_{-0.01}$	...	...	11900	+4.04	0.3	M, x
39.....	G265.5536−03.9951[b]	A5/7 V	73461	0.38	4.78	103^{+20}_{-20}	$0.69^{+0.04}_{-0.04}$	...	...	7200	+4.34	0.6	M, m, c
40.....	G269.5873−05.8882[b]	G0 V	74534	0.43	8.12	53^{+10}_{-10}	$0.87^{+0.01}_{-0.01}$	...	...	6030	+4.39	1.0	M
41.....	G285.8890+01.2948[b]	G8 IV	92643	0.39	7.64	28^{+5}_{-5}	$0.36^{+0.02}_{-0.02}$	...	...	5250	+4.49	0.3	M, c
42.....	G295.3770−02.6386[b]	G2 V	101530	0.31	4.50	43^{+10}_{-10}	$0.10^{+0.01}_{-0.00}$	...	...	5770	+4.49	0.8	M
43.....	G322.6930+00.0572[c]	F7/G0	136591	0.44	7.13	133^{+25}_{-25}	$0.31^{+0.03}_{-0.03}$	...	...	6030	+4.39	0.4	G, v
44.....	G339.4392−00.7791[b]	A0/1 IV/V	151228	0.26	4.48	293^{+45}_{-45}	$1.56^{+0.09}_{-0.09}$	...	...	8200	+4.29	0.5	G
45.....	G339.7415−00.1904[b]	A0	151017	0.26	3.07	758^{+115}_{-115}	$0.52^{+0.03}_{-0.03}$	...	...	9520	+4.14	0.7	G
46.....	G340.0517+00.6687[b]	B8	150625	1.05	16.77	348^{+55}_{-55}	$1.86^{+0.11}_{-0.11}$	...	...	11900	+4.04	0.5	G, e
47.....	G348.5129−00.1121[c]	G0 V	155826	0.52	11.40	18^{+5}_{-5}	$0.41^{+0.04}_{-0.04}$	...	...	6030	+4.39	0.6	M, p, c

NOTES.—Col. (1): Table number. Col. (2): GLIMPSE Catalog ID. Col. (3): Spectral type. Col. (4): HD number. Col. (5): $E(K-[8.0])$. Col. (6): Significance of excess. Col. (7): Spectrophotometric distance. Col. (8): Visual extinction. Col. (9): Best-fit blackbody model temperature for excess. Col. (10): Best-fit infrared luminosity. Col. (11): Effective temperature for the adopted Kurucz (1993) model. Col. (12): log g for the adopted Kurucz model. Col. (13): Radial distance between optical and IR source positions. Col. (14): Other comments: G: GLIMPSE source; M: *MSX* source; e: emission-line star; v: variable star; n: star in nebula; m: multiple stars (from SIMBAD database); o: Oudmaijer et al. (1992) star; p: previous mid-IR spectral work; x: *ROSAT* X-ray source; c: Clarke et al. (2005) star; g: group I designation.

[a] The model fit is marginal and model flux is below [24].

[b] There are no data available for $\lambda > 8$ μm.

[c] This *MSX* star is shown to have a false A-band or [8.0] excess; see text.

[d] This star is a known Be star with the excess arising from a circumstellar shell.

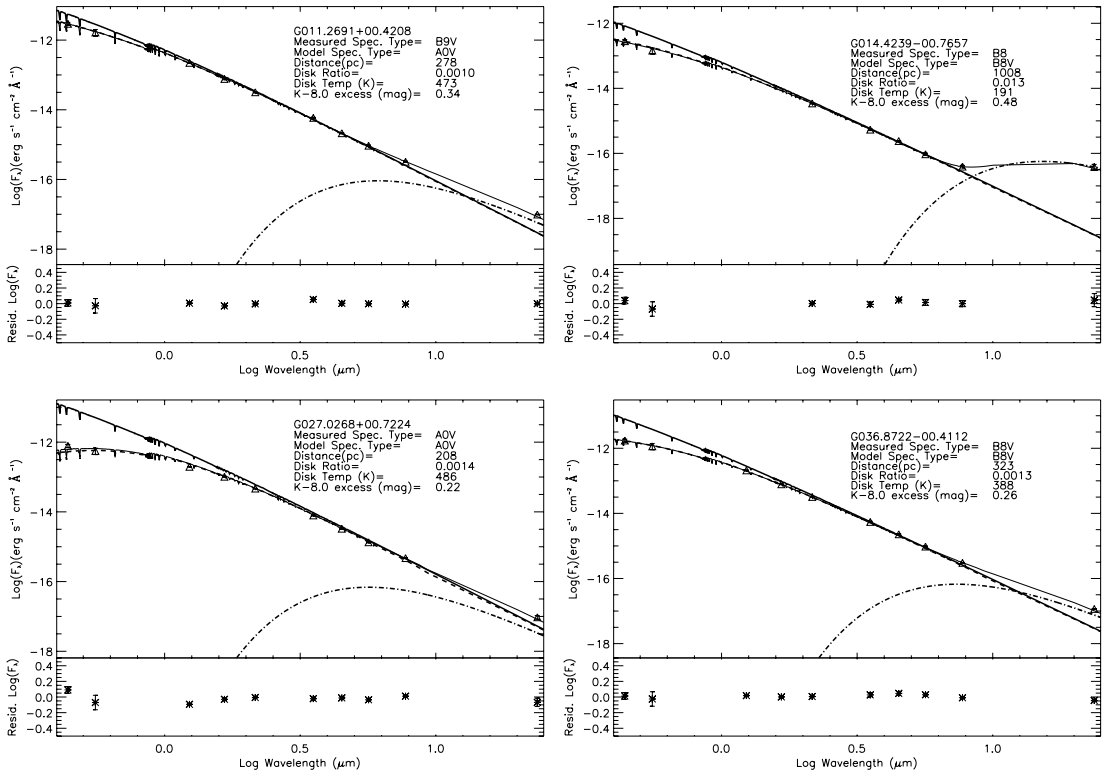

FIG. 9.—*Top left*: SED of the mid-IR excess B9 V star G011.2691+00.4208. The Kurucz model atmosphere is shown by the thick solid line, the model atmosphere with applied extinction is the dashed line, the dot-dashed line is the blackbody representing the disk, and the thin solid line is the extinguished model atmosphere before the addition of the blackbody component. This source is well modeled by a single blackbody component. *Top right*: SED of the mid-IR excess B8 star G014.4239−00.7657. This star is well modeled by a single-temperature blackbody. *Bottom left*: SED of the A0 V star G027.0268+00.7224. The star is adequately modeled by a single-temperature blackbody. *Bottom right*: SED of the B8 V star G036.8722−00.4112. This source is well modeled by a single-temperature blackbody.

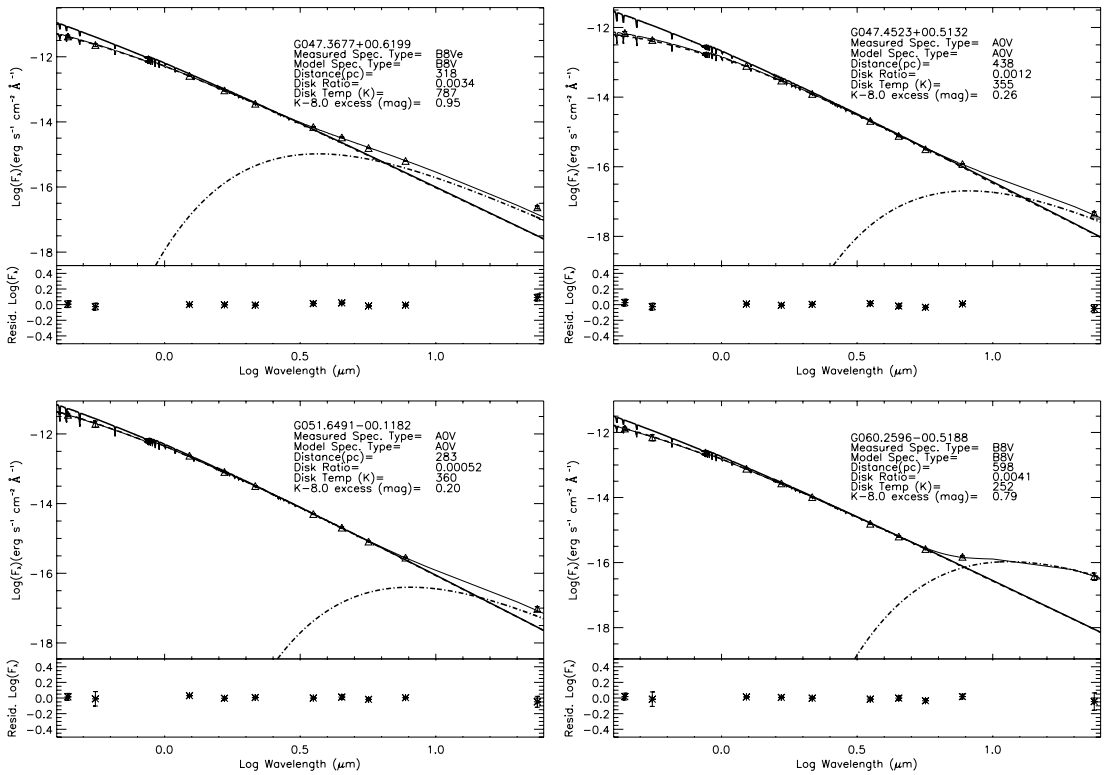

FIG. 10.—*Top left*: SED of the B8 Ve star G047.3677+00.6199. The source is poorly fitted at [24]. *Top right*: SED of the A0 V star G047.4523+00.5132. This star is well fitted by a single-temperature blackbody. *Bottom left*: SED of the A0 V star G051.6491−00.1182. This star is well fitted by a single-temperature blackbody. *Bottom right*: SED of the B8 V star G060.2596−00.5188. The SED of this star is adequately modeled with an additional single-temperature blackbody.

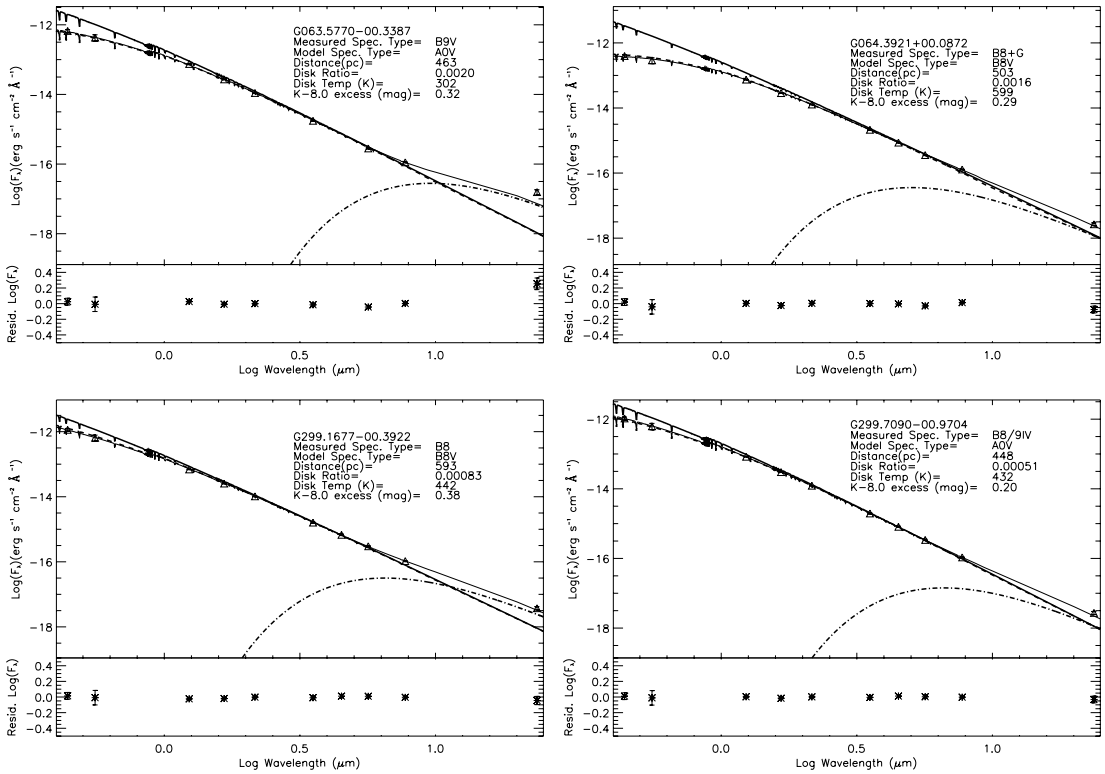

FIG. 11.—*Top left*: SED of the B9 V star G063.5770−00.3387. The model is deficient at [24]. *Top right*: SED of the B8+G star G064.3921+00.0872. The measurements are well fitted by a single-temperature blackbody. *Bottom left*: SED of the B8 star G299.1677−00.3922. This source is well modeled by a single-temperature blackbody. *Bottom right*: SED of the B8/9 IV star G299.7090−00.9704. The model adequately fits the observed fluxes.

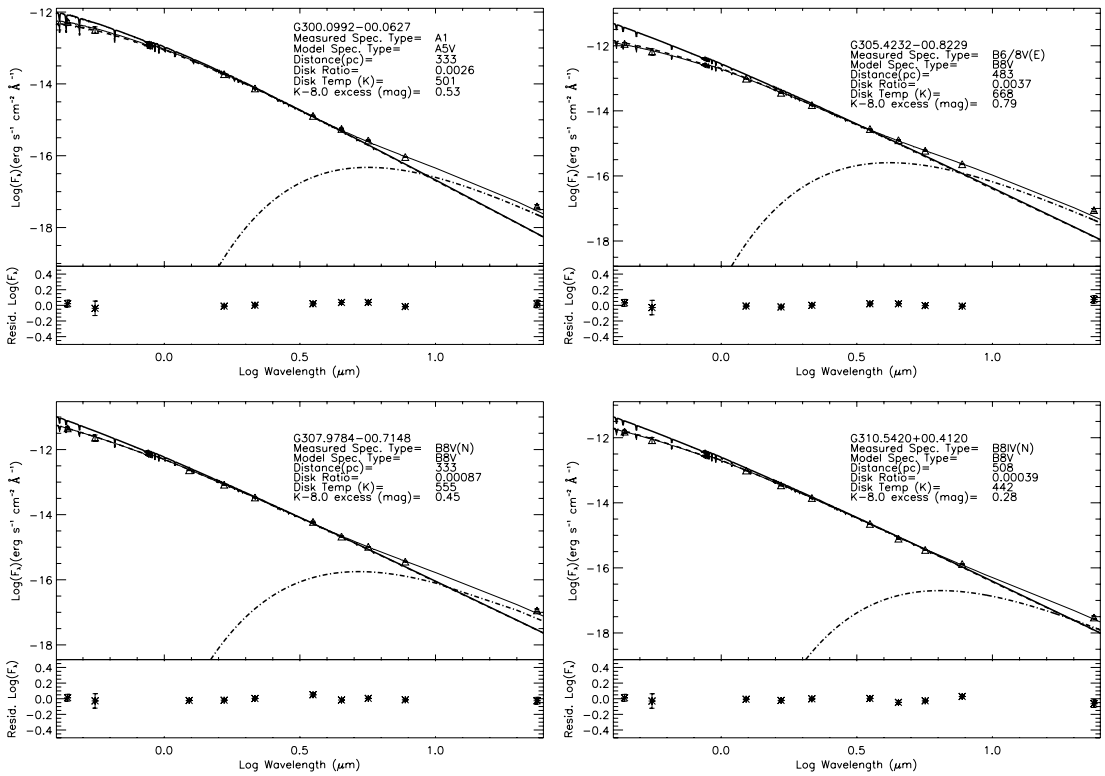

FIG. 12.—*Top left*: SED of the A1 star G300.0992−00.0627. The model fits the observed measurements. *Top right*: SED of the B6/8 V(E) star G305.4232−00.8229. The model is deficient for the [24] measurement. *Bottom left*: SED of the B8 V(N) star G307.9784−00.7148. This star is well modeled with an additional single-temperature blackbody. *Bottom right*: SED of the B8 IV(N) star G310.5420+00.4120. The model for this star fits the observed measurements.

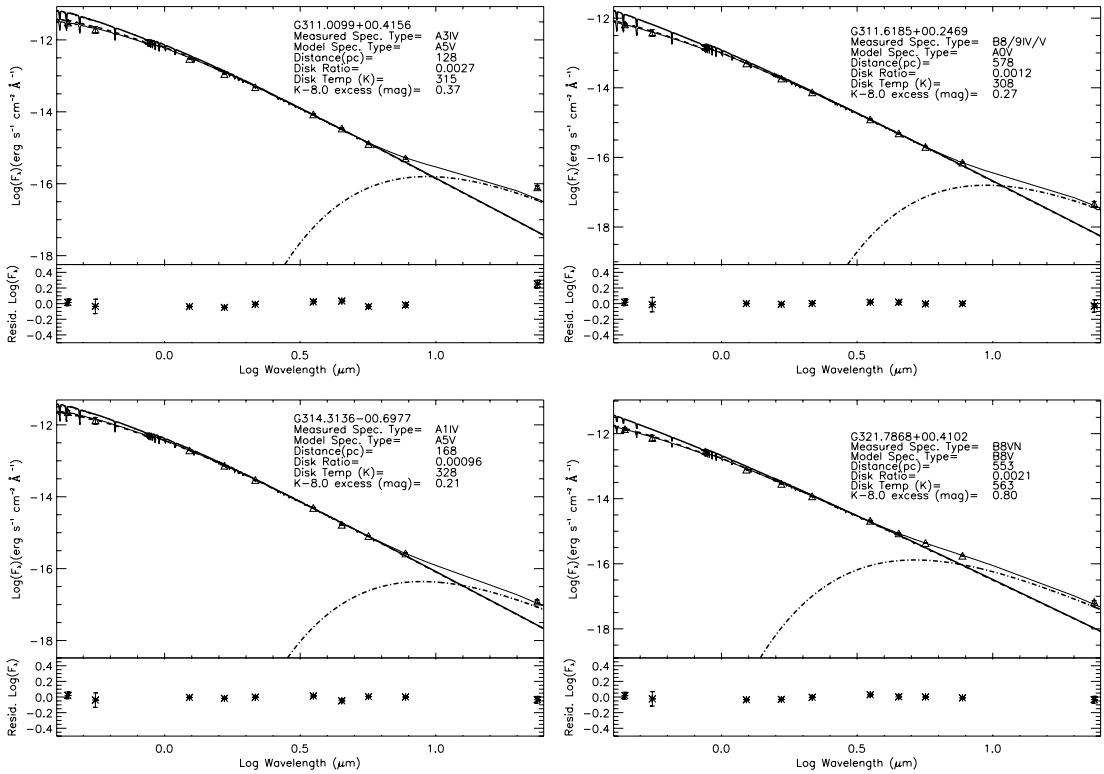

FIG. 13.—*Top left*: SED of the A3 IV star G311.0099+00.4156. The model is deficient at [24]. *Top right*: SED of the B8/9 IV/V star G311.6185+00.2469. This star is well modeled with an additional single-temperature blackbody. *Bottom left*: SED of the A1 IV star G314.3136−00.6977. This star is well modeled with an additional single-temperature blackbody. *Bottom right*: SED of the B8 VN star G321.7868+00.4102. The star is well modeled at [24].

accretion from their circumstellar disks, whereas debris disks should not exhibit accretion characteristics. Three of the six stars with $L_{\rm IR}/L_* \leq 10^{-3}$ exhibit Balmer emission. If the emission-line classification in the SIMBAD database for these sources is reliable, then this signature of ongoing accretion would imply a pre–main-sequence circumstellar disk despite the small fractional infrared luminosity. Four of the six stars that have $L_{\rm IR}/L_* \geq 0.05$ also exhibit Balmer emission, supporting the existence of pre–main-sequence circumstellar disks as the origins of their excesses. Of the remaining 14 stars with $10^{-3} < L_{\rm IR}/L_* < 10^{-2}$, 6 have Balmer emission suggesting ongoing accretion from a circumstellar disk. Given the heterogeneous nature of the spectral information compiled in SIMBAD, stars with very weak Balmer emission (e.g., weak-line T Tauri stars or more massive equivalents) may not have been classified as such in the database. Therefore, we caution that the fraction of emission-line sources in our sample is best regarded as a lower limit. Only 4 of the 21 sources without 24 μm detections exhibit Balmer emission. Approximately half of the sources that were modeled have Balmer emission, regardless of fractional infrared luminosity. In summary, fully one-third of sources identified as having mid-IR excesses also exhibit Balmer emission.

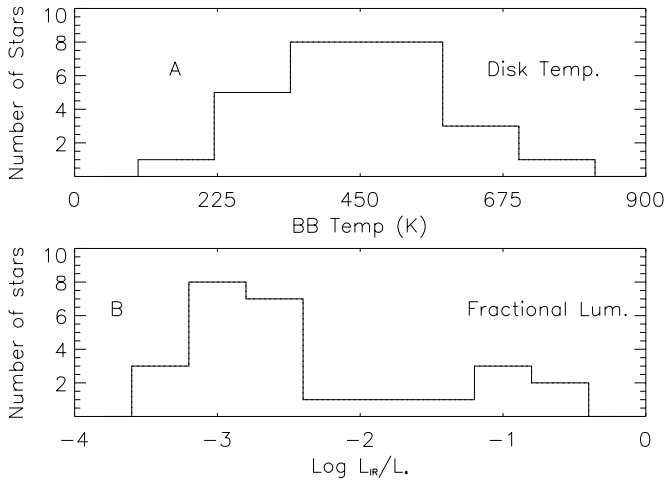

FIG. 14.—Histograms of (*a*) disk temperature and (*b*) fractional infrared luminosity. The distribution of disk temperatures is broadly peaked at ~450 K, but temperatures are found between ~190 and 800 K. The majority of stars have fractional infrared luminosities between 10^{-3} and 10^{-2}. However, there is still a sizable population with fractional infrared luminosities greater than 10^{-2}, including the probable Class II protostars.

Figure 15 is an intercomparison of $E(K-[8.0])$, fractional infrared luminosity, and disk temperature for the 26 modeled sources. Diamonds are GLIMPSE and *MSX* stars lacking evidence of emission lines. Triangles are emission-line GLIMPSE and *MSX* stars. Figure 15*a* plots the modeled $L_{\rm IR}/L_*$ versus the modeled blackbody temperatures, Figure 15*b* shows $L_{\rm IR}/L_*$ versus $E(K-[8.0])$, and Figure 15*c* shows temperature versus $E(K-[8.0])$. In all three panels there is a distinct grouping of six objects that have high fractional infrared luminosities >0.05, large $E(K-[8.0]) > 2$, and temperatures >400 K. This grouping is noted in Table 7 in column (15) by "g" and in Figure 15 as "Group I." All six stars in this group are *MSX* sources and have near-IR excesses ($H-K > 0.3$), and four of them exhibit emission lines. There are four known T Tauri and Herbig Ae/Be stars in this group.

In Figure 15*a*, emission-line stars are found exclusively at temperatures >430 K, and, with three exceptions, non–emission-line stars have temperatures <430 K. Emission-line sources also

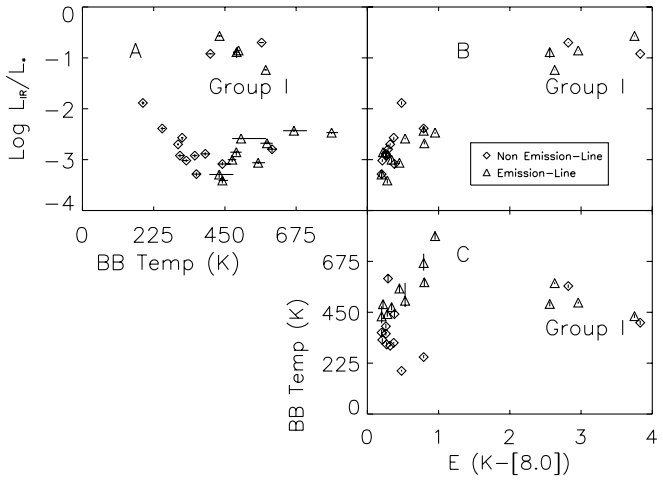

FIG. 15.—Plots of $E(K - [8.0])$, fractional infrared luminosity, and disk temperature for mid-IR excess objects later than B8. Diamonds are GLIMPSE and *MSX* stars without emission lines. Triangles are emission-line GLIMPSE and *MSX* stars. Emission-line and non–emission-line sources show a strong correlation between L_{IR}/L_* and $E(K - [8.0])$. The correlation arises because both measurements are an indicator of extraphotospheric excess.

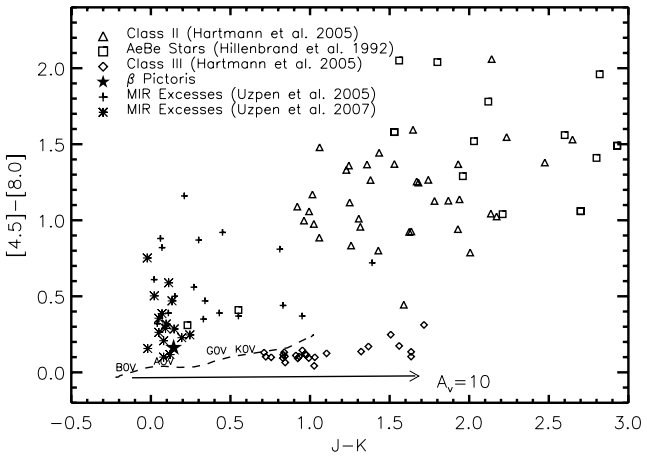

FIG. 16.—Infrared color-color diagram, *Spitzer* 4.5 − 8.0 μm vs. 2MASS $J - K$ showing the loci of Class II protostars (*triangles*), Class III protostars (*diamonds*), Ae/Be stars (*squares*), our sample of mid-IR excess sources from Uzpen et al. (2005) (*plus signs*), and stars with IRAC measurements and [24] detections from this sample (*asterisks*). There is a clear gap between Class II protostars, Class III protostars, and the main-sequence stars. Our samples from Uzpen et al. (2005) and this paper partially bridge this gap. A filled star marks the position of β Pictoris, a prototype debris disk object. The solid line shows the reddening vector for 10 mag of visual extinction. The dashed line marks the main sequence.

show a correlation between L_{IR}/L_* and T when group I sources are excluded. Such a correlation might arise physically if the hottest disks are also youngest and most luminous with the disks closest to the parent stars. The observed correlation between T and L_{IR}/L_* is consistent with an evolutionary progression as the inner disk is cleared of materials (e.g., Strom et al. 1989).

Figure 15*b* shows a correlation between L_{IR}/L_* and $E(K - [8.0])$. This correlation is a consequence of the fact that both quantities are measures of the extraphotospheric excess, the former encompassing all wavelengths and the latter only the [8.0] measurement. That is, objects with large [8.0] excesses must also have large fractional excesses overall. The distribution of $E(K - [8.0])$ is bimodal with group I objects, by definition, having $E(K - [8.0]) > 2$ and the other 20 sources having $E(K - [8.0]) < 1$. The absence of objects with intermediate $E(K - [8.0])$ is likely to be a consequence of selection criteria, stemming from the relative sensitivities and spatial coverage of the *MSX* and GLIMPSE surveys. The limited sensitivity of *MSX* necessarily means that only nearby objects with large 8 μm excesses and detections at wavelengths $\lambda > 8$ μm are included. In fact, group I sources lie at an average distance of $\sim$100 pc, while the other sources are more distant. GLIMPSE, although more sensitive than the *MSX* Galactic Plane Survey, did not include many of the nearby star-forming regions where young stars with large $E(K - [8.0])$ would preferentially reside.

Figure 16 is a color-color diagram, *Spitzer* $[4.5] - [8.0]$ versus 2MASS $J - K$ showing the loci of Class II protostars, Class III protostars, the sample of mid-IR excess sources from Uzpen et al. (2005), and stars with IRAC measurements and [24] detections from this sample. A filled star marks the position of β Pictoris, a prototype debris disk object. The reddening vector is shown for 10 mag of visual extinction. The main sequence is labeled by the dashed line. We adopt the *MSX* A-band measurement in lieu of an [8.0] measurement for the Class II sources from Hillenbrand et al. (1992). For a selected sample of stars we compared GLIMPSE [8.0] and *MSX* A measurements and found that they agreed within 0.1 mag. This error is comparable to the uncertainty in estimating the [8.0] flux by interpolation between K and *MSX* band A. Two Hillenbrand et al. (1992) stars fall in a similar region of color space as our mid-IR excess sources. These are B0–B3 stars from their group III objects, which are classified as young diskless early B stars with excesses attributable to free-free emission. The Class II and III sources from Hartmann et al. (2005) are only late-type stars. There is a clear gap between Class II protostars, Class III protostars, and main-sequence stars. Our samples from this paper and Uzpen et al. (2005) appear to partially bridge this gap. The location of our sample in color space is consistent with the identification of these sources as either late-stage protostars or massive debris disks.

The stars known to have emission are more likely to be pre–main-sequence rather than main-sequence sources and may be in a short-lived transitional state between primordial and debris disks. Further analysis of both emission-line and non–emission-line sources is necessary to understand their evolutionary status and relationship to one another. Mid-IR spectral analysis of the stars in Table 7 would reveal whether the 10 μm silicate feature is present and would be a useful tool in the characterization of mid-IR excesses around main-sequence stars. The absorption (embedded protostar), emission (pre–main sequence), or lack of the 10 μm silicate feature (debris disk) is loosely related to the evolutionary progression of a circumstellar disk (Kessler-Silacci et al. 2005). However, the debris disks studied by Kessler-Silacci et al. (2005) contained debris disks that only exhibited far-IR excesses. β Pictoris, a mid-IR debris disk system, does have a 10 μm silicate emission feature (Weinberger et al. 2003). A useful comparison would be to determine whether this sample of mid-IR excess systems also exhibits a 10 μm silicate emission feature. Detection of gas signatures would also reveal whether these sources are late-stage transitional disks or debris disks. Identification of PAH features in spectra would reveal insight into the nature of the excess, indicating possible circumstellar or interstellar origins. Scattered light observations and resolution of the putative disks would rule out the possibility that the excesses originate in interstellar rather than circumstellar grains (Kalas et al. 2002). Moór et al. (2006) studied a sample of the highest fractional infrared luminosity debris disks and found that they are young, having ages less than 100 Myr. Age measurements

of our sample would allow these objects to be placed within an evolutionary sequence.

5.3. *Individual Sources*

G007.2369+01.4894 (HD 163296) is a well-studied pre–main-sequence star present in over 200 papers, and we place it in group I. It is classified as an A1 V star with a *Hipparcos* distance of 122^{+16}_{-13}. This star has been studied in mid-IR spectroscopy papers such as van Boekel et al. (2005) and Kessler-Silacci et al. (2005). Van Boekel et al. (2005) derive a continuum temperature of 461 K, which is near our temperature of 493^{+4}_{-5} K. In comparison, Oudmaijer et al. (1992) derived a color temperature of 220 K for this source. The presence of crystalline enstatite indicates dust processing in the circumstellar disk. Enstatite is a processed mineral and is made in a circumstellar disk via silicate reactions. We determined $L_{\rm IR}/L_*$ at $0.14^{+0.002}_{-0.002}$, which is consistent with its pre–main-sequence classification.

G008.3752−03.6697 (HD 167905) is an *MSX* source with group I designation that is also listed in Oudmaijer et al. (1992). This F3 V star has an *IRAS* excess with "good"-quality measurements at 12 and 25 μm and "low"-quality measurements at 60 and 100 μm. Oudmaijer et al. (1992) found a temperature of 480 K for the color excess. We find a temperature for the excess to be 566^{+7}_{-8} K when utilizing the *MSX* data. We measured $L_{\rm IR}/L_*$ for this star at $0.20^{+0.004}_{-0.005}$. Given the warmer temperature and larger fractional infrared luminosity, this star is likely pre–main sequence.

G047.3677+00.6199 (HD 180398; Fig. 10, *top left*) is classified as a B8 Ve star and found in the GLIMPSE catalog. The model fit for this source at [24] is below the measured source. In this source, the magnitude of the excess increases with wavelength. An additional cooler disk component may be necessary to fully fit the observed fluxes at all wavelengths.

G063.5770−00.3387 (HD 339086; Fig. 11, *top left*) is a B9 V star in the GLIMPSE sample. This source is located in a small region of extended emission. The model for this source at [24] is below the measurement. A possible explanation is the addition of flux from the extended source to the measurement. An alternate explanation is that an additional cooler disk component may be necessary to fit the observed flux at [24].

G229.4514+01.0145 (HD 58647) is listed as an emission-line star in the SIMBAD database, and we place it in group I. This star is classified as B9 V and its *Hipparcos* distance is 277^{+78}_{-60} pc. This *MSX* source is also an *IRAS* source and has good-quality 12, 25, and 60 μm measurements and low-quality 100 μm measurements. Oudmaijer et al. (1992) measured a color temperature of 650 K for this star, while we measured a blackbody temperature of 579^{+4}_{-5} K. This source has also been investigated for CO emission in Dent et al. (2005), who were only able to place upper limits on the CO intensity. The fractional infrared luminosity is $0.058^{+0.001}_{-0.001}$, smaller than typical for a pre–main-sequence star, but this star has a near-IR excess. This star may be at the end of its pre–main-sequence phase.

G257.6236+00.2459 (HD 72106) is listed as an A0 IV star but is also listed as a multiple or double star in the SIMBAD database. *Hipparcos* parallax places this star at a distance of 288^{+202}_{-84} pc. This *MSX* source and group I member has appeared in numerous *IRAS* far-IR excess searches (e.g., Oudmaijer et al. 1992). This source has good-quality *IRAS* 12, 25, and 60 μm measurements with a low-quality 100 μm measurement, and Oudmaijer et al. (1992) measured the color temperature to be 250 K, while we measured the temperature at 404^{+9}_{-10} K. Given the additional longer wavelength data used by Oudmaijer et al. (1992), it is not unexpected that they derived a lower temperature. We measured $L_{\rm IR}/L_* = 0.12^{+0.002}_{-0.002}$ for this source. The southern component of the binary system is identified as a Herbig Ae/Be source (Vieira et al. 2003). Schütz et al. (2005) note that the mid-IR spectrum lacks small amorphous silicates, has large amorphous silicates, and contains crystalline silicates forsterite and enstatite. The later species are evidence of grain processing in the circumstellar disk. They also note that the mid-IR spectrum is similar to solar system comets and this object is interesting in the context of planet formation.

G294.1242+01.4656 (HD 101412), a B9/A0 V star, is listed as an emission-line star in the SIMBAD database. This *MSX* source and group I member has appeared in numerous *IRAS* papers searching for far-IR excesses (e.g., Oudmaijer et al. 1992). This source is also listed as a possible Herbig Ae/Be star. The star has good-quality 12 and 25 μm data and intermediate-quality 60 and 100 μm data. The color temperature derived for this source in Oudmaijer et al. (1992) is only 170 K. Given the longer wavelength data used by Oudmaijer et al. (1992), it is not unexpected that we derived a higher temperature of 433^{+8}_{-8} K using only the mid-IR data available from *MSX*. This source has also been investigated using mid-IR spectroscopy in van Boekel et al. (2003, 2005), who measure the temperature of the mid-IR continuum to be 425 K, consistent with our temperature. This source also exhibits a large mass fraction of large grains, and the majority of the crystalline grain component is enstatite. In comparing the mid-IR spectrum to HD 163296, HD 101412 has a larger fraction of grains in large grains and more crystalline grains in enstatite form. We determined $L_{\rm IR}/L_*$ at $0.27^{+0.004}_{-0.006}$, which is consistent with the pre–main-sequence classification.

G305.4232−00.8229 (HD 114757; Fig. 12, *top right*) is a B6/8 V(E) star. This source is inadequately fitted at [24]. This deficiency at longer wavelength may imply the need for an additional cool disk component.

G311.0099+00.4156 (HD 121808; Fig. 13, *top left*) is a GLIMPSE star classified as A3 IV. The model is deficient at [24]. This deficiency may imply the need for an additional cool disk component in the SED. The star is also in a region of bright extended background emission. The model deficiency at [24] could also be explained by excess background emission at [24].

G347.3777+04.2010 (HD 152404) is a T Tauri–type star in the Upper Centaurus Lupus (Chen et al. 2005) and in group I. It is classified as an F5 V star with a *Hipparcos* distance of 145^{+38}_{-25} pc. In addition to having good-quality 12, 25, and 60 μm *IRAS* data, this source also has *Spitzer* 24 and 70 μm measurements. Acke & van den Ancker (2004) measured this *MSX* source to have the 9.7 μm silicate feature to be in emission using *ISO*. We determined $L_{\rm IR}/L_*$ at $0.13^{+0.02}_{-0.03}$, which is consistent with its pre–main-sequence classification.

G040.9995−00.0423 (HD 177904) is an *MSX* source that exhibits an excess at band A. This source was also detected in GLIMPSE, G040.9998−00.0429, and MIPSGAL. This source does not exhibit an excess at [8.0] or [24]. This source is, therefore, a probable false excess in the A band.

G042.9876+00.4201 (HD 178479) is a GLIMPSE source classified as a B8 V star. This star has photospheric measurements at [24], and the cause of the [8.0] excess may be due to PAH contamination.

G054.5163+02.4470 (HD 182293) is an *MSX* source exhibiting an excess at both A and C bands. The 2MASS *K* measurement is flagged "U" and provides only an upper limit. In modeling the excess for this star, we find that if all three 2MASS measurements are included, the fractional infrared luminosity exceeded unity in all models. However, if only the *K* measurement was included in the disk models, the fractional infrared excess was $\sim 10^{-1}$. Given

the poor reliability of the IR measurements for this source, we do not model it.

G056.7848+00.8671 (HD 334593) is an *MSX* source also found in the GLIMPSE catalog as G056.7850+00.8668. This source is detected strongly at [24] and does not exhibit an excess based on the GLIMPSE measurement SED. There is a nearby object seen in the [24] image, 6″ separation, which is probably the source of the additional flux in the larger *MSX* beam.

G201.9029−01.9739 (HD 44783) is a B8 VN source listed as a Be star (e.g., Neiner et al. 2005). The excess for this source is attributed to a circumstellar shell rather than circumstellar disk.

G322.6930+00.0572 (HD 136591) is the only late-type star in GLIMPSE that exhibits an $E(K - [8.0])$. This star does not exhibit a [24] excess. This star is listed as a variable in SIMBAD. The [8.0] excess may be due to interstellar PAH emission or offset between the 2MASS and IRAC measurements due to variability.

G348.5129−00.1121 (HD 155826) is a G0 V *MSX* source at 31^{+1}_{-2} pc. It appears in numerous papers as a Vega-like system, including Dent et al. (2005), Jayawardhana et al. (2001), Sylvester et al. (1996), and Aumann (1985). Lisse et al. (2002) observed this source with the Long Wavelength Spectrometer camera on Keck and found an extremely red object in the field of this star. They note that the red source is either a highly reddened carbon star or a Class II YSO and that HD 155826 should no longer be considered a Vega-like source.

5.4. *Mid-IR Excess Fraction among MSX and GLIMPSE Stars*

Based on stars detectable at *IRAS* and *ISO* sensitivities, at least 15% of nearby A–K main-sequence stars have dusty debris disks (Lagrange et al. 2000; Backman & Paresce 1993). Plets & Vynckier (1999) found the excess fraction for both main-sequence stars and their descendants to be ∼13% ± 10%, and Bryden et al. (2006) found the excess fraction for main-sequence FGK stars with $L_{\rm IR}/L_* > 10^{-4}$ to be 2% ± 2%. The statistics for disk fraction from both of these studies rely exclusively on longer wavelength data, such as 24 and 60 μm. Aumann & Probst (1991) investigated nearby main-sequence stars using 12 μm measurements from *IRAS* and found that less than 0.5% of stars exhibit a mid-infrared excess. Fajardo-Acosta et al. (2000) investigated 296 main-sequence B9 through M stars and found that nearly 3% of their sample had a mid-infrared excess at *IRAS* 12 μm.

Given the large number of sources investigated in this study, we can place constraints on the fraction of stars that exhibit mid-IR excesses. Of the 1203 main-sequence Tycho-2 stars in GLIMPSE, 1024 are later than B8. We found that 19 GLIMPSE sources with V or IV luminosity classes exhibited mid-IR excesses (omitting HD 178479, a false excess source). There are seven additional GLIMPSE objects with unknown luminosity class that exhibit mid-IR excesses (omitting HD 136591, a false excess source). These two omitted sources represent the expected number of false sources due to source correlation errors and statistical deviations. For the *MSX* sample, we found that of the 872 main-sequence stars, 785 are of spectral type later than B8. We found that 16 of the sources of luminosity class V or IV exhibited mid-IR excesses (omitting HD 155826, HD 177904, and HD 334593, which are false excess sources).

Omitting the six probable pre–main-sequence objects (group I), the stars found to be false excess sources, and requiring luminosity classification, we determine the fraction of stars showing mid-IR excesses to be $1.9^{+0.4}_{-0.5}$% for the GLIMPSE sample and 1.3% ± 0.4% for the *MSX* sample. If we remove stars with main-sequence classifications listed as emission-line stars or X-ray sources, there are 10 remaining GLIMPSE sources, 8 of which have confirmed excesses at [24]. If we perform the same procedure on the *MSX* sample and remove the emission-line and pre–main-sequence sources, eight stars remain. Given these numbers, we estimate the fraction of main-sequence stars that exhibit a mid-IR but not a near-IR excess, at 1.0% ± 0.3% for the GLIMPSE sample and 1.0% ± 0.4% for the *MSX* sample. These statistics might be considered an upper limit if some of the sample stars turn out to have infrared excesses owing to free-free emission or contamination from a field object. On the other hand, this statistic might be considered a lower limit if luminosity class is determined for the seven additional GLIMPSE sources and they are shown to be main sequence. This might also be considered a lower limit if we include emission-line sources.

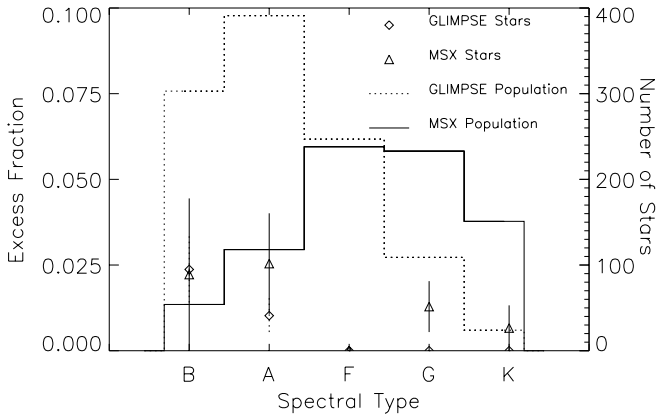

FIG. 17.— Plot of excess fraction (on the left abscissa) vs. spectral type for 1024 sources from GLIMPSE (*diamonds*) and 785 from *MSX* (*triangles*). The histograms show the number of main-sequence GLIMPSE objects (*dashed*) and *MSX* objects (*solid*) (numbered on the right abscissa) contained in the Tycho-2 Spectral Catalog. For spectral types B8–K the average fraction of main-sequence stars with mid-IR excesses is 1.0% ± 0.3%, varying slightly by type.

Figure 17 shows the fraction of stars exhibiting mid-IR excesses on the left abscissa versus spectral type (*symbols*). Only non–emission-line, non–X-ray–emitting stars having known luminosity class are included. For both the GLIMPSE and *MSX* samples, the fraction of excess stars changes with spectral type, with GLIMPSE having the largest fraction of excess stars among B stars and *MSX* among A stars. For the *MSX* sample, the excess fraction for B, A, and G stars is similar at ∼2%. K stars show a smaller excess fraction, and there are no F stars with excesses. The GLIMPSE sample also shows a decrease in excess fraction with later spectral type. However, there were no F, G, or K stars with an excess in the GLIMPSE sample. The histogram in Figure 17 shows, on the right abscissa, the number of stars in the parent population as a function of spectral type. For example, there were 391 stars in the GLIMPSE sample of spectral type A, and of this subsample, 4 exhibited a mid-IR excess, yielding an excess fraction of 1.0% ± 0.5%.

6. CONCLUSIONS

We investigated stars exhibiting 8 μm mid-IR excesses in the GLIMPSE and *MSX* catalogs. We found 36 probable main-sequence sources that have a mid-infrared excess but no near-infrared excess (omitting HD 136591, HD 155826, HD 177904, HD 178479, and HD 334593). All of these sources lie in a region of mid-IR color space distinct from both main-sequence and Class II and III pre–main-sequence stars. We modeled the properties of the putative circumstellar disks in 20 of the 36 sources. We found putative circumstellar disk temperatures to range from 191 K $< T <$ 787 K. Six stars exhibit fractional infrared luminosities less than or equal to 10^{-3} and are consistent with

having debris disks similar to β Pictoris, although three of them exhibit Balmer emission lines. The majority of our sample (14 stars) have $10^{-3} < L_{\rm IR}/L_* < 10^{-2}$ and are consistent with either transition disks in late-stage protostars or massive debris disks. These objects have fractional infrared luminosities and temperatures between those of β Pic–type debris disk systems ($L_{\rm IR}/L_* \leq 10^{-3}$) and Class II pre–main-sequence systems ($L_{\rm IR}/L_* \simeq 10^{-1}$). We find that the putative circumstellar disk sources that exhibit emission lines have temperatures >430 K, while those that do not exhibit emission lines are almost exclusively <430 K. Excluding probable Class II pre–main-sequence stars, emission-line stars show a correlation between temperature and fractional infrared luminosity. This correlation among mid-IR excess sources might imply an evolutionary progression from high temperature and moderate fractional infrared luminosity to low temperature and small fractional infrared luminosity consistent with inner disk clearing.

We estimate that the incidence of main-sequence stars found within the Tycho-2 Spectral Catalog with mid-IR excesses is $1.0\% \pm 0.3\%$. This statistic varies among spectral types B8–K in both the GLIMPSE and *MSX* surveys, with B stars exhibiting an excess fraction of $2.4\% \pm 1.0\%$ in GLIMPSE and $2.2\% \pm 2.2\%$ in *MSX*. The mid-IR excess fraction among A stars is smaller in the GLIMPSE sample, $1.0\% \pm 0.5\%$, but statistically equivalent to the *MSX* sample, $2.5\% \pm 1.5\%$. We did not find any main-sequence F stars, in either survey, that exhibited a mid-IR excess (<0.4%). In the *MSX* sample, $1.3\% \pm 0.7\%$ of main-sequence G stars exhibited a mid-IR excess, while only $0.7\% \pm 0.7\%$ of K stars exhibited a mid-IR excess. The GLIMPSE sample did not contain any main-sequence G or K stars that exhibited a mid-IR excess (<1.0% and <4.1%, respectively). The statistics of field FGK main-sequence stars are consistent with those of Bryden et al. (2006) determined using longer wavelengths. The mean excess fraction measured here is much lower than the 15%–20% of main-sequence stars that exhibit far-IR excesses at $\lambda \geq 60$ μm (Lagrange et al. 2000). The rarity of main-sequence stars that exhibit mid-IR but not near-IR excesses suggests that this stage of star formation is short lived, and further investigation of these sources will help identify their place in the evolutionary process of star and planet formation.

We would like to thank Lynne Hillenbrand for her helpful discussion. We would like to thank Dylan Semler for his assistance observing at WIRO. We acknowledge the comments from a critical referee that inspired significant improvements to this manuscript. Support for this work, part of the *Spitzer Space Telescope* Legacy Science Program, was provided by NASA through contracts (institutions) 1224653 (UW), 1225025 (BU), 1224681 (UMd), 1224988 (SSI), 1242593 (UCB), 1253153 (UMn), 1253604 (UWy), 1256801 (UWW) by the Jet Propulsion Laboratory, California Institute of Technology under NASA contract 1407. B. U. acknowledges support from a NASA Graduate Student Researchers Program Fellowship, grant NNX06AI28H. This research has made use of the SIMBAD database, operated at CDS, Strasbourg, France. This publication makes use of data products from the Two Micron All Sky Survey, which is a joint project of the University of Massachusetts and the Infrared Processing and Analysis Center/California Institute of Technology, funded by the National Aeronautics and Space Administration and the National Science Foundation.

REFERENCES

Acke, B., & van den Ancker, M. E. 2004, A&A, 426, 151
Artymowicz, P. 1996, in The Role of Dust in the Formation of Stars, ed. H. U. Kaufl & R. Siebenmorgen (New York: Springer), 137
Aumann, H. H. 1985, PASP, 97, 885
Aumann, H. H., & Probst, R. G. 1991, ApJ, 368, 264
Aumann, H. H., et al. 1984, ApJ, 278, L23
Backman, D. E., Gillett, F. C., & Witteborn, F. C. 1992, ApJ, 385, 670
Backman, D. E., & Paresce, F. 1993, in Protostars and Planets III, ed. E. Levy & J. I. Lunine (Tucson: Univ. Arizona Press), 1253
Barlow, M. J., & Cohen, M. 1977, ApJ, 213, 737
Barrado y Navascués, D. 1998, A&A, 339, 831
Barrado y Navascués, D., Stauffer, J. R., Song, I., & Caillault, J-P. 1999, ApJ, 522, L53
Baud, B., et al. 1984, ApJ, 278, L53
Benjamin, R., et al. 2003, PASP, 115, 953
Bryden, G., et al. 2006, ApJ, 636, 1098
Dent, W. R. F., Greaves, J. S., & Coulson, I. M. 2005, MNRAS, 359, 663
Chen, C. H., & Jura, M. 2001, ApJ, 560, L171
Chen, C. H., et al. 2005, ApJ, 634, 1372
Clarke, A. J., Oudmaijer, R. D., & Lumsden, S. L. 2005, MNRAS, 363, 1111
Cohen, M., Hammersley, P. L., & Egan, M. P. 2000, AJ, 120, 3362
Cutri, R. M. 2003, 2MASS All-Sky Catalog of Point Sources (Pasadena: IPAC)
Drilling, J. S., & Landolt, A. U. 2000, in Astrophysical Quantities, ed. A. N. Cox (4th ed.; New York; Springer), 381
Egan, M. P., et al. 2003, The *Midcourse Space Experiment* Point Source Catalog, Version 2.3, Air Force Research Laboratory Tech. Rep. AFRL-VS-TR-2003-1589
Fajardo-Acosta, S. B., Beichman, C. A., & Cutri, R. M. 2000, ApJ, 538, L155
Fazio, G. G., et al. 2004, ApJS, 154, 10
Gehrz, R. D., Hackwell, J. A., & Jones, T. W. 1974, ApJ, 191, 675
Hartmann, L., et al. 2005, ApJ, 629, 881
Hernández, J., Briceño, C., Calvet, N., Hartmann, L., Muzerolle, J., & Quintero, A. 2006, ApJ, 652, 472
Hillenbrand, L. A., Strom, S. E., Vrba, F. J., & Keene, J. 1992, ApJ, 397, 613
Hog, E., et al. 2000, A&A, 355, L27
Indebetouw, R., et al. 2005, ApJ, 619, 931
Jayawardhana, R., Fisher, R. S., Telesco, C. M., Piña, R. K., Barrado y Navascués, D., Hartmann, L. W., & Fazio, G. G. 2001, AJ, 122, 2047
Kalas, P., Graham, J. R., Beckwith, S. V. W., Jewitt, D. C., & Lloyd, J. P. 2002, ApJ, 567, 999
Kessler-Silacci, J. E., Hillenbrand, L. A., Blake, G. A., & Meyer, M. R. 2005, ApJ, 622, 404
Kurucz, R. 1993, Kurucz CD-ROM 13, ATLAS9 Stellar Atmospheres Programs and 2 km/s Grid (Cambridge: SAO)
Lada, C. J., & Wilking, B. A. 1984, ApJ, 287, 610
Lagrange, A.-M., Backman, D. E., & Artymowicz, P. 2000, in Protostars and Planets IV, ed. V. Mannings, A. P. Boss, & S. S. Russell (Tucson: Univ. Arizona Press), 639
Li, A., & Draine, B. T. 2001, ApJ, 554, 778
Lisse, C., et al. 2002, ApJ, 570, 779
Mannings, V., & Barlow, M. J. 1998, ApJ, 497, 330
Megeath, S. T., Hartmann, L., Luhman, K. L., & Fazio, G. G. 2005, ApJ, 634, L113
Meyer, M. R., Backman, D. E., Weinberger, A. J., & Wyatt, M. C. 2007, in Protostars and Planets V, ed. B. Reipurth, D. Jewitt, & K. Keil (Tucson: Univ. Arizona Press), 573
Moór, A., Ábrahám, P., Derekas, A., Kiss, Cs., Kiss, L. L., Apai, D., Grady, C., & Henning, Th. 2006, ApJ, 644, 525
Neiner, C., Hubert, A.-M., & Catala, C. 2005, ApJS, 156, 237
Oudmaijer, R. D., van der Veen, W. E. C. J., Waters, L. B. F. M., Trams, N. R., Waelkens, C., & Engelsman, E. 1992, A&AS, 96, 625
Plets, H., & Vynckier, C. 1999, A&A, 343, 496
Price, S. D., Egan, M. P., Carey, S. J., Mizuno, D. R., & Kuchar, T. A. 2001, AJ, 121, 2819
Reach, W. T., et al. 2005, PASP, 117, 978
Rieke, G. H., et al. 2004, ApJS, 154, 25
Schütz, O., Meeus, G., & Sterzik, M. F. 2005, A&A, 431, 175
Sicilia-Aguilar, A., et al. 2006, ApJ, 638, 897
Silverstone, M. D., et al. 2006, ApJ, 639, 1138
Strom, K. M., Strom, S. E., Edwards, S., Cabrit, S., & Skrutskie, M. F. 1989, AJ, 97, 1451
Su, K. Y. L., et al. 2005, ApJ, 628, 487

Sylvester, R. J., Skinner, C. J., Barlow, M. J., & Mannings, V. 1996, MNRAS, 279, 915
Uzpen, B., et al. 2005, ApJ, 629, 512
van Boekel, R., Min, M., Waters, L. B. F. M., de Koter, A., Dominik, C., van den Ancker, M. E., & Bouwman, J. 2005, A&A, 437, 189
van Boekel, R., Waters, L. B. F. M., Dominik, C., Bouwman, J., de Koter, A., Dullemond, C. P., & Paresce, F. 2003, A&A, 400, L21
Vieira, S. L. A., Corradi, W. J. B., Alencar, S. H. P., Mendes, L. T. S., Torres, C. A. O., Quast, G. R., Guimarães, M. M., & da Silva, L. 2003, AJ, 126, 2971
Weinberger, A. J., Becklin, E. E., & Zuckerman, B. 2003, ApJ, 584, L33
Werner, M., Fazio, G. G., Rieke, G., Roellig, T., & Watson, D. 2006, ARA&A, 44, 269
Werner, M., Uchida, K. I., Sellgren, K., Marengo, M., Gordon, K. D., Morris, P. W., Houck, J. R., & Stansberry, J. A. 2004, ApJS, 154, 391
Wilking, B. A., Lada, C. J., & Young, E. T. 1989, ApJ, 340, 823
Wright, C. O., Egan, M. P., Kraemer, K. E., & Price, S. D. 2003, AJ, 125, 359
Yamashita, Y., Nariai, K., & Norimoto, Y. 1976, An Atlas of Representative Stellar Spectra (New York: Halsted)
Zuckerman, B. 2001, ARA&A, 39, 549